The modified Myers boundary condition for swirling flow

James R. Mathews*
University of Cambridge, Cambridge, CB3 0WA, UK

Vianney Masson†, Stéphane Moreau‡
Université de Sherbrooke, Sherbrooke, QC J1K 2R1, Canada

Hélène Posson§
Airbus Commercial Aircraft, 316 route de Bayonne, 31060 Toulouse, France

This paper gives a modified Myers boundary condition in swirling flow, which differs from the standard Myers boundary condition by assuming a small but non-zero boundary layer thickness. The new boundary condition is derived and is shown to have the correct quadratic error behaviour with boundary layer thickness and also to agree with previous results when the swirl is set to zero. The boundary condition is then used to analyse the eigenmodes and Green's function in a realistic flow. It is shown that it is essential to model the thickness of the boundary layer properly in order to get accurate results.

Nomenclature

Latin Characters

c_0	Base flow speed of sound
$\widehat{c}_0$	Scaled base flow speed of sound to produce a limit as $y \to \infty$
D_0/Dt	Base flow convective derivative
G_ω	Reduced Green's function at a particular frequency in the duct
g_1, g_2	Solutions to the pressure differential equation with certain boundary conditions
h	Non-dimensionalised inner radius of the duct
i	Imaginary unit
k	Axial wavenumber and eigenmode
k_m^n	A specific acoustic eigenmode indexed by n at a specific azimuthal number m
m	Azimuthal number
P	Fourier transform of pressure pertubation
P_∞	The value of the pressure at the duct wall without a boundary layer
$\widehat{p}_\omega$	Reduced Green's function at a particular frequency in the duct
$\widehat{p}_\omega^m$	Contribution to $\widehat{p}_\omega$ from all acoustic eigenmode at the azimuthal number m
$\widehat{p}_m$	Axial Fourier transform of the m-th azimuthal Fourier series coefficient of $\widehat{p}_\omega$
$\underline{p}$	Total pressure of the flow
p	Pressure perturbation
p_0	Base flow pressure
$\widehat{p}_0$	Scaled base flow pressure to produce a limit as $y \to \infty$
r	Non-dimensionalised radial coordinate
r_m	Non-dimensionalised midspan of the duct

*Research Associate, Department of Engineering, jrm214@cam.ac.uk.
†PhD candidate, Département de Génie Mécanique, vianney.masson@usherbrooke.ca.
‡Professor, Département de Génie Mécanique, stephane.moreau@usherbrooke.ca.
§Research engineer, Airbus Acoustic Department, helene.posson@airbus.com.

t	Time
$U_\theta(r)$	Swirl profile for base flow
$U_x(r)$	Shear profile for base flow
(U, V, W)	Fourier transform of velocity pertubations
$\widetilde{U}, \widetilde{W}$	Scaled Fourier transforms of U and W; $\widetilde{U} = U/\delta$, $\widetilde{W} = W/\delta$
$(\underline{u}, \underline{v}, \underline{w})$	Total velocities of the flow (in x, r and θ directions respectively)
(u, v, w)	Velocity perturbations
(u_0, v_0, w_0)	Base flow velocities
V_∞	The value of the normal velocity at the duct wall without a boundary layer
x	Non-dimensionalised axial coordinate
$\boldsymbol{x} = (x, r, \theta)$	Cylindrical coordinates in the duct
$\boldsymbol{x_0} = (x_0, r_0, \theta_0)$	Source position in the duct
y	inner axial coordinate, $r = h + \delta y$ or $r = 1 - \delta y$
Z	Complex impedance of acoustic lining at duct walls
Z_{eff}	Effective impedance at the duct wall to replicate a boundary layer
Greek Characters	
α	Parameter controlling exponential boundary layer, $\alpha \propto 1/\delta$
γ	Ratio of specific heat capacities
δ	Boundary layer thickness
$\delta(f)$	Dirac delta
δI	Integrals needed to calculate the effective impedance
δJ	Integrals needed to calculate the effective impedance
ε	Displacement thickness of the boundary layer
θ	Circumferential coordinate
Λ	Function in differential equation for pressure, $\Lambda = 0$ defines critical layer
$\underline{\rho}$	Density of the total flow
ρ	Density perturbation
ρ_0	Base flow density
$\widehat{\rho}_0$	Scaled base flow density to produce a limit as $y \to \infty$
Υ	Function in differential equation for pressure
ω	Non-dimensionalised frequency
Other Characters	
$\mathcal{A}$, $\mathcal{B}$, $\mathcal{C}$	Coefficients of second order differential equation for pressure P
$\mathcal{F}$	Sixth order differential operator acting on pressure pertubation p in acoustic analogy
$\mathcal{K}_m^{\pm}$	Set of all acoustic downstream/upstream eigenmodes for a specific azimuthal number m
$\mathcal{R}$, $\mathcal{T}$	Differential operators in the acoustic analogy
$\mathbb{S}$	Source terms in acoustic analogy
$\mathcal{U}_\theta$	Function in differential equation for pressure which depends only on swirl U_θ
$\mathcal{W}$	Wrońskian of g_1 and g_2
Other notation	
Double dagger ‡	Quantities with dimension
Subscript $_0$	Base flow functions
Subscript $_{\text{nbl}}$ or superscript $^{\text{nbl}}$	Flow parameters without a boundary layer
Underlined	Total function, sum of perturbation and base flow

I. Introduction

Environmental concerns such as noise pollution, greenhouse gas emissions and fuel efficiency are changing the way modern aeroengines are designed and used. In 2001 ACARE[1] set environmental targets for 2020, such as reducing the effective perceived noise by 50% and reducing fuel and carbon dioxide emissions by 50%, both compared to the 2000 levels. Flightpath[2] 2050 sets even stronger goals for 2050 to further reduce the environmental concern from air travel. These targets have resulted in a trend in aeroengine design towards ultra high bypass ratio (UHBR) turbofans, with joint European projects such as Clean Sky and ENOVAL currently researching this area.

One method of controlling and reducing the noise in the turbofan is to fit acoustic lining on nacelle walls, which absorbs some of the sound. In UHBR engines, the inlet treated area will be reduced and the relative importance of the interstage liner will increase. These liners often have a honeycomb-perforated sheet structure, and can be characterised and modelled by an impedance Z. The boundary condition for the acoustic lining is then given by $p/v = Z$, where p and v are the pressure and normal velocity perturbations. This boundary condition is only valid when the normal velocity is zero on the surface of the lining, so in viscous fluid. Often, it is more convenient to ignore the viscous effects of the perturbed flow and instead assume the flow satisfies the Euler equations rather than the Navier–Stokes equations.

The boundary condition then needs to be modified, and is generally referred to as the Myers[3] or Ingard-Myers[4] boundary condition, and is derived by matching the fluid and solid normal displacement. This has been the standard boundary condition that has been used in nearly all studies regarding the acoustic propagation through the aeroengine. Recent theoretical evidence by Brambley[5] and experimental evidence by Renou & Aurégan[6] have shown that the Myers boundary condition is not producing the correct behaviour for sound attenuation.

It is often assumed that the Myers boundary condition is the limit of an infinitely thin boundary layer, and it was shown independently by Eversman & Beckemeyer[7] and Tester[8] that this is the case with no swirling flow. However, it was shown in Masson et al.[9] that it is not the correct limit for an infinitely thin boundary layer for swirling flow, with an additional term relating to centrifugal force present. To get a more accurate boundary condition which behaves correctly, the boundary layer thickness must be considered as non-zero. It was shown in Gabard,[10] in the case of non-swirling flow, that using an infinitely thin boundary layer compared to a boundary layer of the correct thickness can lead to significant errors when predicting sound attenuation.

One way of modelling the flow with a finite boundary layer thickness is to fully resolve the flow and just use the boundary condition $p/v = Z$, however this can be very expensive computationally. Instead, we use an asymptotic method which gives an effective boundary condition which we can apply for a flow without the boundary layer. This method was considered by Brambley[11] for non-swirling flow, and latter extended to be more accurate in Khamis & Brambley[12] by considering the asymptotics at second order rather than first order. Rienstra & Darau[13] also considered a similar boundary condition to Brambley at first order, as did Myers & Chuang[14] and Joubert.[15] All of these modified Myers boundary conditions (for non-swirling flow) then had the correct stability properties and were well-posed, as opposed to the original Myers condition.

Recently, it has become more important to consider the swirling flow, such as for understanding the complex interaction between the rotor and stator in the interstage region and better assess the role of the interstage liner. Studies such as Posson & Peake[16] and Mathews & Peake[17] have considered the effect of the swirling flow on the eigenmodes and acoustic Green's function, although only using the Myers boundary condition. To make these studies more relevant, the modified Myers boundary condition for swirling flow is calculated in the present paper, in a similar way to previous studies with no swirl.

This paper is laid out as follows. In Section II the geometry of the problem, governing equations and the corresponding acoustic analogy are considered. In Section III the new modified Myers boundary condition is derived in swirling flow. Both the inner and outer solutions to the asymptotic problem are derived and then matched, which allows for the computation of the boundary condition at both the inner duct wall and outer duct wall. In Section IV it is shown that in the limit of no swirl, our new boundary condition reduces to the boundary condition given in Brambley[11] and Khamis & Brambley.[12] In Section V the modified Myers boundary condition is shown to have the correct quadratic error behaviour with boundary layer thickness, and shown to be more more accurate than the corrected Myers boundary condition from Masson et al.[9] compared to the fully resolved boundary layer. In Section VI the new modified Myers boundary condition is considered in the simplified case of a linear boundary layer, while the extension of the boundary condition from Section III to an arbitrary swirling flow is also derived. Finally, in Section VII the effect of the new boundary condition is considered on the eigenmodes and Green's function for a realistic swirling flow between the rotor and stator.

II. Geometry and acoustic analogy

The aeroengine is modelled as an infinite annular duct. Let the inner and outer duct walls be given by $r^\ddagger = h^\ddagger$ and $r^\ddagger = d^\ddagger$ respectively, where the double dagger $\ddagger$ represents dimensional coordinates. All distances are made dimensionless by $d^\ddagger$, so that the inner wall lies at $r = h := h^\ddagger/d^\ddagger$ and the outer wall at $r = 1$. Let

$r_m^\ddagger = (h^\ddagger + d^\ddagger)/2$ be the midspan of the duct, and $r_m = (h+1)/2$ denote the dimensionless midspan of the duct. All velocities are made dimensionless by the speed of sound at the midspan of the duct, $c_0^\ddagger(r_m^\ddagger)$. The density is made dimensionless by the density at midspan. Finally, time is made dimensionless by $d^\ddagger/c_0^\ddagger(r_m^\ddagger)$ and all frequencies by $c_0^\ddagger(r_m^\ddagger)/d^\ddagger$. The use of the speed of sound at midspan to define non-dimensional speeds, time and frequencies instead of values at the tip is so that the non-dimensionalisation is unaffected by the choice of the flow behaviour near the walls (presence and type of boundary layers).

A cylindrical coordinate system is used, with x the axial coordinate, r the radial coordinate and θ the azimuthal coordinate. Let $\underline{\boldsymbol{u}} = (\underline{u}, \underline{v}, \underline{w})$, $\underline{\rho}$ and $\underline{p}$ be the total velocity, the total density and the total pressure of air, with $\underline{u}$, $\underline{v}$ and $\underline{w}$ being the velocity components in the x, r and θ directions respectively. The total flow (underlined) is split into an inviscid base flow (subscript $_0$) and some small perturbations, so that:

$$(\underline{u}, \underline{v}, \underline{w}, \underline{\rho}, \underline{p}) = (u_0, v_0, w_0, \rho_0, p_0) + (u, v, w, \rho, p). \tag{1}$$

The total flow is assumed to satisfies the non-linearised Euler equations

$$\frac{\partial \underline{\rho}}{\partial t} + \boldsymbol{\nabla} \cdot (\underline{\rho}\underline{\boldsymbol{u}}) = 0, \tag{2}$$

$$\underline{\rho}\left(\frac{\partial \underline{\boldsymbol{u}}}{\partial t} + \underline{\boldsymbol{u}} \cdot \boldsymbol{\nabla}\underline{\boldsymbol{u}}\right) + \boldsymbol{\nabla}\underline{p} = 0. \tag{3}$$

The fluid is assumed to be a perfect gas, which then satisfies the energy equation

$$\frac{\partial \underline{p}}{\partial t} + \underline{\boldsymbol{u}} \cdot \boldsymbol{\nabla}\underline{p} + \gamma \underline{p}(\boldsymbol{\nabla} \cdot \underline{\boldsymbol{u}}) = 0, \tag{4}$$

where γ is the ratio of specific heat capacities ($\gamma = 1.4$ for air). Finally, the flow is assumed homentropic, so the entropy is constant. The real perturbations or fluctuations may not necessarily be inviscid, but any inviscid effects will be introduced as a source term in the acoustic analogy of Section III.C.

A. Swirling base flow in a duct with a boundary layer

The swirling base flow is assumed non-viscous and homentropic so the entropy is constant. The mean velocity of the base flow is assumed of the form

$$(u_0, v_0, w_0) = (U_x(r), 0, U_\theta(r)), \tag{5}$$

where $U_x(r)$ and $U_\theta(r)$ are freely chosen. The speed of sound density and pressure are then deduced from the Euler equations and the gas thermodynamic relations. This choice of base flow is representative of the swirling mean flow in the interstage region of a turbofan. The speed of sound c_0 is given by

$$c_0^2(r) = 1 + (\gamma - 1)\int_{r_m}^{r} \frac{U_\theta^2(s)}{s}\mathrm{d}s, \tag{6}$$

while the density is given by

$$\rho_0(r) = [c_0^2(r)]^{1/(\gamma-1)}, \tag{7}$$

and finally the pressure is given by

$$p_0(r) = \frac{1}{\gamma} - \int_{r}^{r_m} \frac{\rho_0(s)U_\theta^2(s)}{s}\mathrm{d}s, \tag{8}$$

where $p_0(r_m) = 1/\gamma$ is computed using the Newton-Laplace equation, which relates the speed of sound, density and pressure.

B. Swirling base flow in a duct without a boundary layer

We denote the flow without the boundary layer with a subscript or superscript "nbl". The velocities are given by

$$(u_0, v_0, w_0) = (U_x^{\mathrm{nbl}}(r), 0, U_\theta^{\mathrm{nbl}}(r)) \tag{9}$$

with pressure $p_{\mathrm{nbl}}(r)$, density $\rho_{\mathrm{nbl}}(r)$ and speed of sound $c_{\mathrm{nbl}}(r)$. These are given by

$$c_{\mathrm{nbl}}^2(r) = 1+(\gamma-1)\int_{r_m}^{r} \frac{(U_\theta^{\mathrm{nbl}})^2(s)}{s}\mathrm{d}s, \quad \rho_{\mathrm{nbl}}(r) = [c_{\mathrm{nbl}}^2(r)]^{1/(\gamma-1)} \text{ and } p_{\mathrm{nbl}}(r) = \frac{1}{\gamma} - \int_{r}^{r_m} \frac{\rho_{\mathrm{nbl}}(s)(U_\theta^{\mathrm{nbl}})^2(s)}{s}\mathrm{d}s. \tag{10}$$

C. Acoustic analogy

In Posson & Peake[16] an acoustic analogy was derived for the pressure perturbation. The analogy was derived by considering an exact rearrangement of the Navier–Stokes equations, such that we got a single, sixth-order linear differential equation for pressure on the left-hand side. On the right-hand side is a source term $\mathbb{S}$ which includes the non-linear effects, viscous effects and the rotor-stator geometry. The analogy is given by

$$\mathcal{F}(p) = \mathbb{S}, \tag{11}$$

where the differential operator $\mathcal{F}$ is (using the notation from Mathews & Peake[17])

$$\begin{aligned}\mathcal{F} = \left(\frac{1}{c_0^2}\frac{{D_0}^2}{Dt^2} - \frac{\partial^2}{\partial x^2} - \frac{1}{r^2}\frac{\partial^2}{\partial\theta^2}\right)\mathcal{R}^2 + \left(\frac{1}{r}\frac{D_0}{Dt} - U_x'\frac{\partial}{\partial x} - \left(\frac{U_\theta}{r^2} + \frac{U_\theta'}{r}\right)\frac{\partial}{\partial\theta}\right)\mathcal{R}\mathcal{T} \\ + \mathcal{R}\frac{D_0}{Dt}\frac{\partial}{\partial r}\mathcal{T} - \frac{D_0}{Dt}\left[2U_x'\frac{\partial}{\partial x}\frac{D_0}{Dt} + 2\left(\frac{U_\theta}{r}\right)'\frac{\partial}{\partial\theta}\frac{D_0}{Dt} + \mathcal{U}_\theta'\right]\mathcal{T},\end{aligned} \tag{12}$$

where

$$\mathcal{R} = \frac{{D_0}^2}{Dt^2} + \mathcal{U}_\theta, \quad \mathcal{T} = -\frac{D_0}{Dt}\frac{\partial}{\partial r} - \frac{2U_\theta}{r^2}\frac{\partial}{\partial\theta} + \frac{U_\theta^2}{rc_0^2}\frac{D_0}{Dt}, \quad \frac{D_0}{Dt} = \frac{\partial}{\partial t} + U_x\frac{\partial}{\partial x} + \frac{U_\theta}{r}\frac{\partial}{\partial\theta}, \tag{13}$$

and

$$\mathcal{U}_\theta(r) = \frac{2U_\theta(r)}{r}\left(\frac{U_\theta(r)}{r} + U_\theta'(r)\right). \tag{14}$$

The source term $\mathbb{S}$ is given in Posson & Peake.[16] To calculate the pressure perturbation for the linearised Euler equations we simply solve $\mathcal{F}(p) = 0$.

D. Fourier transform

For the most part, it will be more useful to consider the Fourier transforms in time and axial direction and Fourier series in the azimuthal direction of the pressure and velocity perturbations, given by

$$\{u, v, w, p\}(r, x, \theta, t) = \int\sum_m\int\{U(r), V(r), W(r), P(r)\}e^{\mathrm{i}kx}\mathrm{d}k e^{\mathrm{i}m\theta}e^{-\mathrm{i}\omega t}\mathrm{d}\omega, \tag{15}$$

namely, here and throughout the time dependence of the flow is chosen of the form $\exp(-\mathrm{i}\omega t)$. After Fourier transforming $\mathcal{F}(p) = 0$ we find a linear, second order ordinary equation acting on P, as given in Posson & Peake[16] and Mathews & Peake.[17] It is given by

$$\mathcal{A}(r,k)\frac{\mathrm{d}^2P}{\mathrm{d}r^2}(r;k) + \mathcal{B}(r,k)\frac{\mathrm{d}P}{\mathrm{d}r}(r;k) - \mathcal{C}(r,k)P(r;k) = 0, \tag{16}$$

where

$$\mathcal{A}(r,k) = (\mathcal{U}_\theta(r) - \Lambda^2(r,k))\Lambda^2(r,k), \tag{17}$$

$$\mathcal{B}(r,k) = \Lambda^2(r,k)\left[(\mathcal{U}_\theta(r) - \Lambda^2(r,k))\left(\frac{1}{r} - \frac{\rho_0'(r)}{\rho_0(r)}\right) + \left(\Lambda^2(r,k) - \mathcal{U}_\theta(r)\right)'\right], \tag{18}$$

and

$$\mathcal{C}(r,k) = (\mathcal{U}_\theta - \Lambda^2)^2\left(\frac{\Lambda^2}{c_0^2} - k^2 - \frac{m^2}{r^2}\right) + \Upsilon(\mathcal{U}_\theta - \Lambda^2)\left[\Upsilon - \Lambda\left(\frac{1}{r} - \frac{\rho_0'}{\rho_0}\right)\right] - \Upsilon[\Lambda(\Lambda^2 - \mathcal{U}_\theta)]' + \Lambda(\Lambda^2 - \mathcal{U}_\theta)\Upsilon', \tag{19}$$

with

$$\Lambda(r,k) = kU_x(r) + \frac{mU_\theta(r)}{r} - \omega \quad \text{and} \quad \Upsilon(r,k) = -\frac{U_\theta^2(r)\Lambda(r,k)}{rc_0^2(r)} + \frac{2mU_\theta(r)}{r^2}, \tag{20}$$

with primes denoting derivatives with respect to r.

Instead of having one governing equation for the pressure, the problem can equivalently be writen as two coupled governing equations for pressure and normal velocity, which are given by

$$\frac{\mathrm{d}P}{\mathrm{d}r}(r;k) + \frac{\Upsilon(r,k)}{\Lambda(r,k)}P(r;k) = \mathrm{i}\rho_0(r)\frac{\left(\mathcal{U}_\theta(r) - \Lambda^2(r,k)\right)}{\Lambda(r,k)}V(r;k) \tag{21}$$

and

$$\frac{\mathrm{d}V}{\mathrm{d}r}(r;k) + \left(\frac{1}{r} - \frac{\Upsilon(r,k) + \Lambda'(r,k)}{\Lambda(r,k)}\right)V(r;k) = \frac{1}{\mathrm{i}\rho_0(r)\Lambda(r,k)}\left(\frac{\Lambda(r,k)^2}{c_0^2(r)} - k^2 - \frac{m^2}{r^2}\right)P(r;k). \tag{22}$$

As a final alternative, the problem can also be described as a set of four coupled differential equations, for the pressure and the three velocity components, which are calculated directly from Fourier transforming the linearised momentum equation and a combined linearised mass and energy equation. They are given by

$$\frac{\mathrm{i}\Lambda P}{c_0^2} + V\frac{\rho_0 U_\theta^2}{rc_0^2} + \rho_0\left[\frac{\mathrm{i}mW}{r} + \mathrm{i}kU + \frac{V}{r} + \frac{\mathrm{d}V}{\mathrm{d}r}\right] = 0, \tag{23}$$

$$\rho_0\left[\mathrm{i}\Lambda U + V\frac{\mathrm{d}U_x}{\mathrm{d}r}\right] + \mathrm{i}kP = 0, \tag{24}$$

$$\rho_0\left[\mathrm{i}\Lambda V - \frac{2U_\theta}{r}W\right] + \frac{\mathrm{d}P}{\mathrm{d}r} - \frac{U_\theta^2}{rc_0^2}P = 0, \tag{25}$$

$$\rho_0\left[\mathrm{i}\Lambda W + V\left(\frac{U_\theta}{r} + \frac{\mathrm{d}U_\theta}{\mathrm{d}r}\right)\right] + \frac{\mathrm{i}mP}{r} = 0. \tag{26}$$

E. Acoustic lining of the duct

The duct walls are either hard walls or acoustically treated with liners of uniform properties, although they may be different at each duct wall. To mathematically model the acoustic lining in the frequency domain, the impedances $Z_h^\ddagger, Z_1^\ddagger \in \mathbb{C}$ of the liner at the duct walls are introduced. The impedances are made dimensionless at the midspan of the duct, such that $Z_j = Z_j^\ddagger/(\rho_0^\ddagger(r_m^\ddagger)c_0^\ddagger(r_m^\ddagger))$. The case of hard walls corresponds to an impedance of $Z_j = \infty$.

After Fourier transforming, the boundary conditions become

$$\frac{P(1)}{V(1)} = Z_{\mathrm{eff}}^1 \text{ and } \frac{P(h)}{V(h)} = -Z_{\mathrm{eff}}^h, \tag{27}$$

where Z_{eff}^j depends on the choice of boundary condition and the thickness of the boundary layer, which we summarise below.

1. Flow with boundary layer

If the flow has a boundary layer with $U_\theta = U_x = 0$ at the duct walls, then we simply have $Z_{\mathrm{eff}}^h = Z_h$ and $Z_{\mathrm{eff}}^1 = Z_1$.

2. Myers boundary condition

In the Myers[3] boundary condition, the fluid and solid normal displacement are matched. The effective impedance is then given by

$$Z_{\mathrm{eff}}^r = \frac{\omega}{\omega - kU_x^{\mathrm{nbl}}(r) - \frac{mU_\theta^{\mathrm{nbl}}(r)}{r}}Z_r, \tag{28}$$

for $r = h$ and $r = 1$. For hard walls we have $Z_r \to \infty$, hence $Z_{\mathrm{eff}}^r \to \infty$ and the boundary condition at the duct wall becomes $V(h) = V(1) = 0$. It was shown independently by Eversman & Beckemeyer[7] and Tester[8] that this was the correct limit in the case of an infinitely thin boundary layer with no swirl. However, it was shown in Masson et al.[9] that this was not the correct limit for an infinitely thin boundary layer in swirling flow.

3. Corrected Myers boundary condition in swirl

In Masson et al.[9] it was shown that a correct choice of effective impedance is

$$Z^h_{\text{eff}} = \frac{\omega}{\omega - kU^{\text{nbl}}_x(h) - \frac{mU^{\text{nbl}}_\theta(h)}{h}} \left(Z + \frac{\mathrm{i}}{h\omega}\rho_{\text{nbl}}(h) \left(U^{\text{nbl}}_\theta(h)\right)^2 \right), \tag{29}$$

and

$$Z^1_{\text{eff}} = \frac{\omega}{\omega - kU^{\text{nbl}}_x(1) - mU^{\text{nbl}}_\theta(1)} \left(Z - \frac{\mathrm{i}}{\omega}\rho_{\text{nbl}}(1) \left(U^{\text{nbl}}_\theta(1)\right)^2 \right), \tag{30}$$

which was shown to produce the correct limit as the boundary layer became infinitely thin.

III. Deriving the modified Myers boundary condition in swirl

To derive the modified Myers boundary condition we need to relate how the flow is behaving without a boundary layer at the duct wall and how the flow is behaving with a boundary layer at the duct wall. This will then allow us to calculate the effective impedance Z_{eff} for the flow without a boundary layer in terms of Z and the boundary layer. To relate the two different flows, we will calculate the outer solution (without a boundary layer) at the duct wall, calculate the inner solution (with a boundary layer) near the duct wall and then match the two solutions. We will assume the boundary layer thickness is δ. In this section we will assume the flow away from the boundary layer is constant.

A. Outer solution

We begin by looking at the outer solutions for $P(r)$ and $V(r)$ in a duct. It will be sufficient to calculate how $P(r)$ and $V(r)$ relate to each other, and to be able to calculate their derivatives in terms of $P(r)$ and $V(r)$.

1. Derivatives of $V(r)$ and $P(r)$

From the coupled equations for pressure and normal velocity in (21) and (22) we can easily calculate that the derivative of the pressure is given by

$$\boxed{\frac{\mathrm{d}P}{\mathrm{d}r}(r) = \mathrm{i}\rho_0(r)\frac{\left(\mathcal{U}_\theta(r) - \Lambda^2(r)\right)}{\Lambda(r)}V(r) - \frac{\Upsilon(r)}{\Lambda(r)}P(r),} \tag{31}$$

and the derivative of pressure is given by

$$\boxed{\frac{\mathrm{d}V}{\mathrm{d}r}(r) = -\left(\frac{1}{r} - \frac{\Upsilon(r) + \Lambda'(r)}{\Lambda(r)}\right)V(r) + \frac{1}{\mathrm{i}\rho_0(r)\Lambda(r)}\left(\frac{\Lambda(r)^2}{c_0^2(r)} - k^2 - \frac{m^2}{r^2}\right)P(r).} \tag{32}$$

2. Taylor expansion

We now consider the outer solution in terms of the flow without the boundary layer, denoted with a subscript or superscript "nbl". We further make the assumption that both U^{nbl}_x and U^{nbl}_θ are constant, and look for the outer solution near the wall at $r = h$. After Taylor expanding We find

$$V_{\text{nbl}}(h+\delta y) = V_{\text{nbl}}(h) + \delta y\frac{\mathrm{d}V_{\text{nbl}}}{\mathrm{d}r}(h) + \mathcal{O}(\delta^2) \text{ and } P_{\text{nbl}}(h+\delta y) = P_{\text{nbl}}(h) + \delta y\frac{\mathrm{d}P_{\text{nbl}}}{\mathrm{d}r}(h) + \mathcal{O}(\delta^2). \tag{33}$$

Letting V^h_∞ and P^h_∞ denote $V_{\text{nbl}}(h)$ and $P_{\text{nbl}}(h)$, we find in terms of the flow without the boundary layer

$$V_{\text{nbl}}(h+\delta y) = V^h_\infty + \delta y\left[\left\{-\frac{1}{h} + \frac{\Upsilon_{\text{nbl}}(h) - \frac{nU^{\text{nbl}}_\theta}{h^2}}{\Lambda_{\text{nbl}}(h)}\right\}V^h_\infty + \frac{1}{\mathrm{i}\rho_{\text{nbl}}(h)\Lambda_{\text{nbl}}(h)}\left\{\frac{\Lambda_{\text{nbl}}(h)^2}{c^2_{\text{nbl}}(h)} - k^2 - \frac{m^2}{h^2}\right\}P^h_\infty\right] + \mathcal{O}(\delta^2) \tag{34}$$

and

$$P_{\text{nbl}}(h+\delta y) = P^h_\infty + \delta y\left[\mathrm{i}\rho_{\text{nbl}}(h)\frac{\left(\mathcal{U}^{\text{nbl}}_\theta(h) - \Lambda^2_{\text{nbl}}(h)\right)}{\Lambda_{\text{nbl}}(h)}V^h_\infty - \frac{\Upsilon_{\text{nbl}}(h)}{\Lambda_{\text{nbl}}(h)}P^h_\infty\right] + \mathcal{O}(\delta^2) \tag{35}$$

where

$$\Lambda_{\rm nbl}(r) = kU_x^{\rm nbl} + \frac{mU_\theta^{\rm nbl}}{r} - \omega \tag{36}$$

and

$$\Upsilon_{\rm nbl}(r) = -\frac{(U_\theta^{\rm nbl})^2\Lambda_{\rm nbl}(r)}{rc_{\rm nbl}^2(r)} + \frac{2mU_\theta^{\rm nbl}}{r^2} \text{ and } \mathcal{U}_\theta^{\rm nbl}(r) = \frac{2(U_\theta^{\rm nbl})^2}{r^2}, \tag{37}$$

To get the solution at the other duct wall we replace h by 1 and δ by $-\delta$.

B. Inner solution

To derive the inner solution, we first make the change of variables $r = h + \delta y$ in the governing equations, and then look for pressure and normal velocity solutions of the form

$$P(y) = P_0(y) + \delta P_1(y) + \mathcal{O}(\delta^2) \quad \text{and} \quad V(y) = V_0(y) + \delta V_1(y) + \mathcal{O}(\delta^2). \tag{38}$$

If we use the four coupled governing equations in (23) to (26) rather than the two coupled differential equations, then we will also need to make the scaling

$$U = \frac{\widetilde{U}}{\delta} \text{ and } W = \frac{\widetilde{W}}{\delta}, \tag{39}$$

and consider

$$\widetilde{U}(y) = \widetilde{U}_0(y) + \delta\widetilde{U}_1(y) + \mathcal{O}(\delta^2), \quad \text{and } \widetilde{W}(y) = \widetilde{W}_0(y) + \delta\widetilde{W}_1(y) + \mathcal{O}(\delta^2). \tag{40}$$

Finally, since the pressure, density and speed of sound all vary with radius due to the swirling flow, it will be necessary to scale them in such a way that the limit as $y \to \infty$ is well defined, which is needed for the matching of the inner and outer solutions. To perform this scaling we multiply ρ_0 and p_0 (and their derivatives) by

$$\frac{\rho_{\rm nbl}(0)}{\rho_{\rm nbl}(y)} = 1 - \delta y\frac{\rho'_{\rm nbl}(h)}{\rho_{\rm nbl}(h)} + \mathcal{O}(\delta^2) \text{ and } \frac{p_{\rm nbl}(0)}{p_{\rm nbl}(y)} = 1 - \delta y\frac{p'_{\rm nbl}(h)}{p_{\rm nbl}(h)} + \mathcal{O}(\delta^2), \tag{41}$$

where the prime denotes differentiation with respect to r. This will then give expression in terms of

$$\widehat{\rho_0}(y) = \frac{\rho_{\rm nbl}(0)\rho_0(y)}{\rho_{\rm nbl}(y)} \text{ and } \widehat{p_0}(y) = \frac{p_{\rm nbl}(0)p_0(y)}{p_{\rm nbl}(y)}, \tag{42}$$

which then have a limit as $y \to \infty$. We also use $\widehat{c_0}(y)$ to denote the speed of sound in a similar way.

1. *Leading order solution*

After performing analysis similar to Masson et al.,[9] and matching to the (constant) leading order outer solution, we find that

$$V_0(y) = \frac{V_\infty^h}{\Lambda_{\rm nbl}(h)}\Lambda_h(y) \text{ and } P_0(y) = P_\infty^h - \frac{\mathrm{i}V_\infty^h}{h\Lambda_{\rm nbl}(h)}\int_y^\infty \widehat{\rho_0}(U_\theta^2)_y \mathrm{d}y, \tag{43}$$

where $\Lambda_h(y) = kU_x(y) + mU_\theta(y)/h - \omega$. We additionally find that

$$\widetilde{U}_0(y) = \mathrm{i}\frac{V_\infty^h}{\Lambda_{\rm nbl}(h)}(U_x(y))_y \text{ and } \widetilde{W}_0(y) = \mathrm{i}\frac{V_\infty^h}{\Lambda_{\rm nbl}(h)}(U_\theta(y))_y, \tag{44}$$

where the subscript y denotes differentiation with respect to y.

2. First order solution

To derive the first order solution we will use the governing equations in (23) to (26), although exactly the same result is derived using the other set of governing equations, and is closer in terms of method to Khamis & Brambley.[12] After making the change of variables $r = h + \delta y$ the differential equations satisfy to first order

$$\frac{\mathrm{i}\Lambda_h P_0}{\widehat{c_0}^2} + V_0\frac{\widehat{\rho_0}U_\theta^2}{h\widehat{c_0}^2} + \widehat{\rho_0}\left[\frac{\mathrm{i}m\widetilde{W_1}}{h} - \frac{\mathrm{i}my\widetilde{W_0}}{h^2} + \mathrm{i}k\widetilde{U_1} + \frac{V_0}{h} + \frac{\mathrm{d}V_1}{\mathrm{d}y}\right] = 0, \tag{45}$$

$$\widehat{\rho_0}\left[\mathrm{i}\Lambda_h\widetilde{U_1} - \frac{\mathrm{i}myU_\theta}{h^2}\widetilde{U_0} + V_1\frac{\mathrm{d}U_x}{\mathrm{d}y}\right] + \mathrm{i}kP_0 = 0, \tag{46}$$

$$\widehat{\rho_0}\left[\mathrm{i}\Lambda_h V_0 - \frac{2U_\theta}{h}\widetilde{W_1} + \frac{2yU_\theta\widetilde{W_0}}{h^2}\right] + \frac{\mathrm{d}P_1}{\mathrm{d}y} - y\frac{\mathrm{d}P_0}{\mathrm{d}y}\frac{\rho'_{\mathrm{nbl}}(h)}{\rho_{\mathrm{nbl}}(h)} - \frac{U_\theta^2}{h\widehat{c_0}^2}P_0 = 0, \tag{47}$$

$$\widehat{\rho_0}\left[\mathrm{i}\Lambda_h\widetilde{W_1} - \frac{\mathrm{i}myU_\theta}{h^2}\widetilde{W_0} + V_1\frac{\mathrm{d}U_\theta}{\mathrm{d}y} + V_0\frac{U_\theta}{h}\right] + \frac{\mathrm{i}mP_0}{h} = 0, \tag{48}$$

where the second to last term in (47) arises due to the scaling in (41).

We use (46) to calculate $\widetilde{U_1}$ in terms of V_1 and known terms from (43) and (44), before using (48) to similarly express $\widetilde{W_1}$ in terms of V_1 and known terms. We then substitute these into (45), which after some simplifications gives a differential equation for V_1 with

$$\frac{\Lambda'_h}{\Lambda_h}V_1 - \frac{\mathrm{d}V_1}{\mathrm{d}y} - \frac{\mathrm{i}}{\widehat{\rho_0}\Lambda_h}\left(\frac{\Lambda_h^2}{\widehat{c_0}^2} - k^2 - \frac{m^2}{h^2}\right)P_0 + \frac{V_\infty^h}{\Lambda_{\mathrm{nbl}}(h)}\left[\frac{\Lambda_h}{h}\left(1 + \frac{U_\theta^2}{\widehat{c_0}^2}\right) - \frac{2mU_\theta}{h^2} + \frac{m}{h^2}(yU_\theta)_y - \frac{myU_\theta}{h^2}\frac{\Lambda'_h}{\Lambda_h}\right] = 0. \tag{49}$$

The solution to this differential equation is then given by

$$V_1 = C_h\Lambda_h(y) - \mathrm{i}\Lambda_h\int_0^y P_0\frac{1}{\widehat{\rho_0}\Lambda_h^2}\left(\frac{\Lambda_h^2}{\widehat{c_0}^2} - k^2 - \frac{m^2}{h^2}\right)\mathrm{d}y - \frac{\Lambda_h}{h}\frac{V_\infty^h}{\Lambda_{\mathrm{nbl}}(h)}\int_0^y\left(1 + \frac{U_\theta^2}{\widehat{c_0}^2}\right)\mathrm{d}y - \frac{2m\Lambda_h}{h^2}\frac{V_\infty^h}{\Lambda_{\mathrm{nbl}}(h)}\int_0^y\frac{U_\theta}{\Omega_h}\mathrm{d}y + \frac{myU_\theta}{h^2\Lambda_{\mathrm{nbl}}(h)}V_\infty^h, \tag{50}$$

where C_h is to be determined. Finally, we write (50) in terms of bounded integrals, which gives

$$\begin{aligned}
V_1 = {} & C_h\Lambda_h - \frac{y\mathrm{i}\Lambda_h}{\rho_{\mathrm{nbl}}(h)c_{\mathrm{nbl}}^2(h)}P_\infty^h + \frac{\mathrm{i}\Lambda_h}{\rho_{\mathrm{nbl}}(h)c_{\mathrm{nbl}}^2(h)}P_\infty^h\int_0^y\left(1 - \frac{P_0}{P_\infty^h}\frac{\rho_{\mathrm{nbl}}(h)c_{\mathrm{nbl}}^2(h)}{\widehat{\rho_0}\widehat{c_0}^2}\right)\mathrm{d}y \\
& + \mathrm{i}y\Lambda_h\frac{k^2 + \frac{m^2}{h^2}}{\rho_{\mathrm{nbl}}(h)\Lambda_{\mathrm{nbl}}^2(h)}P_\infty^h - \mathrm{i}\Lambda_h\frac{k^2 + \frac{m^2}{h^2}}{\rho_{\mathrm{nbl}}(h)\Lambda_{\mathrm{nbl}}^2(h)}P_\infty^h\int_0^y\left(1 - \frac{P_0}{P_\infty^h}\frac{\rho_{\mathrm{nbl}}(h)\Lambda_{\mathrm{nbl}}^2(h)}{\widehat{\rho_0}\Lambda_h^2}\right)\mathrm{d}y \\
& - \frac{y\Lambda_h}{h}\frac{V_\infty^h}{\Lambda_{\mathrm{nbl}}(h)} - \frac{ymU_\theta}{h^2}\frac{V_\infty^h}{\Lambda_{\mathrm{nbl}}(h)} - \frac{y\Lambda_h(U_\theta^{\mathrm{nbl}})^2}{hc_{\mathrm{nbl}}^2(h)}\frac{V_\infty^h}{\Lambda_{\mathrm{nbl}}(h)} + \frac{\Lambda_h(U_\theta^{\mathrm{nbl}})^2}{hc_{\mathrm{nbl}}^2(h)}\frac{V_\infty^h}{\Lambda_{\mathrm{nbl}}(h)}\int_0^y\left(1 - \frac{U_\theta^2c_{\mathrm{nbl}}^2(h)}{(U_\theta^{\mathrm{nbl}})^2\widehat{c_0}^2}\right)\mathrm{d}y \\
& + \frac{2ym\Lambda_hU_\theta^{\mathrm{nbl}}}{h^2\Lambda_{\mathrm{nbl}}^2(h)}V_\infty^h - \frac{2m\Lambda_hU_\theta^{\mathrm{nbl}}}{h^2\Lambda_{\mathrm{nbl}}^2(h)}V_\infty^h\int_0^y\left(1 - \frac{U_\theta\Lambda_{\mathrm{nbl}}(h)}{U_\theta^{\mathrm{nbl}}\Lambda_h}\right)\mathrm{d}y,
\end{aligned} \tag{51}$$

where the integrands are all zero outside of the boundary layer.

We now calculate the pressure term P_1. Using the expression in (47), substituting in $\widetilde{W_1}$ and the known terms from (43) and (44) gives a differential equation for P_1 which involves V_1, and after solving it we find that

$$P_1 = D_h + \int_0^y P_0\left[\frac{U_\theta^2}{h\widehat{c_0}^2} - \frac{2mU_\theta}{h^2\Lambda_h}\right]\mathrm{d}y - \mathrm{i}\frac{V_\infty^h}{\Lambda_{\mathrm{nbl}}(h)}\int_0^y\widehat{\rho_0}\left[\Lambda_h^2 - \frac{2U_\theta^2}{h^2}\right]\mathrm{d}y - \frac{V_\infty^h}{\Lambda_{\mathrm{nbl}}(h)}\int_0^y\mathrm{i}\widehat{\rho_0}\frac{y(U_\theta^2)_y}{h^2}\left(1 - \frac{mU_\theta}{h\Lambda_h} - \frac{(U_\theta^{\mathrm{nbl}})^2}{c_{\mathrm{nbl}}^2(h)}\right)\mathrm{d}y + \int_0^y\frac{\mathrm{i}\widehat{\rho_0}(U_\theta^2)_y}{h\Lambda_h}V_1\mathrm{d}y. \tag{52}$$

We then write (52) in terms of bounded integrals (plus an integral involving V_1) as

$$
\begin{aligned}
P_1 = {} & D_h + \frac{(U_\theta^{\mathrm{nbl}})^2}{hc_{\mathrm{nbl}}^2(h)} P_\infty^h y - \frac{(U_\theta^{\mathrm{nbl}})^2}{hc_{\mathrm{nbl}}^2(h)} P_\infty^h \int_0^y \left(1 - \frac{P_0}{P_\infty^h} \frac{U_\theta^2 c_{\mathrm{nbl}}^2(h)}{(U_\theta^{\mathrm{nbl}})^2 \widehat{c_0}^2}\right) \mathrm{d}y \\
& - \frac{2mU_\theta^{\mathrm{nbl}}}{h^2 \Lambda_{\mathrm{nbl}}(h)} P_\infty^h y + \frac{2mU_\theta^{\mathrm{nbl}}}{h^2 \Lambda_{\mathrm{nbl}}(h)} P_\infty^h \int_0^y \left(1 - \frac{P_0}{P_\infty^h} \frac{U_\theta \Lambda_{\mathrm{nbl}}(h)}{U_\theta^{\mathrm{nbl}} \Lambda_h}\right) \mathrm{d}y \\
& - \mathrm{i}\rho_{\mathrm{nbl}}(h) \Lambda_{\mathrm{nbl}}(h) V_\infty^h y + \mathrm{i}\rho_{\mathrm{nbl}}(h) \Lambda_{\mathrm{nbl}}(h) V_\infty^h \int_0^y \left(1 - \frac{\widehat{\rho_0} \Lambda_h^2}{\rho_{\mathrm{nbl}}(h) \Lambda_{\mathrm{nbl}}^2(h)}\right) \mathrm{d}y \\
& + 2\mathrm{i} \frac{\rho_{\mathrm{nbl}}(h)(U_\theta^{\mathrm{nbl}})^2}{h^2 \Lambda_{\mathrm{nbl}}(h)} V_\infty^h y - 2\mathrm{i} \frac{\rho_{\mathrm{nbl}}(h)(U_\theta^{\mathrm{nbl}})^2}{h^2 \Lambda_{\mathrm{nbl}}(h)} V_\infty^h \int_0^y \left(1 - \frac{\widehat{\rho_0} U_\theta^2}{\rho_{\mathrm{nbl}}(h)(U_\theta^{\mathrm{nbl}})^2}\right) \mathrm{d}y \\
& - \frac{V_\infty^h}{\Lambda_{\mathrm{nbl}}(h)} \int_0^y \mathrm{i}\widehat{\rho_0} \frac{y (U_\theta^2)_y}{h^2} \left(1 - \frac{mU_\theta}{h\Lambda_h} - \frac{(U_\theta^{\mathrm{nbl}})^2}{c_{\mathrm{nbl}}^2(h)}\right) \mathrm{d}y + \int_0^y \frac{\mathrm{i}\widehat{\rho_0} (U_\theta^2)_y}{h\Lambda_h} V_1 \mathrm{d}y.
\end{aligned} \tag{53}
$$

C. Matching

We now match the inner and outer solutions by comparing them at $\mathcal{O}(\delta)$, which allows us to calculate the constants C_h and D_h.

1. *Normal velocity*

As we let $y \to \infty$ in the inner solution of the normal velocity (51), we see that the $\mathcal{O}(y)$ term is given by

$$
y \left[\frac{1}{\mathrm{i}\rho_{\mathrm{nbl}}(h)\Lambda_{\mathrm{nbl}}(h)} \left(\frac{\Lambda_{\mathrm{nbl}}^2}{c_{\mathrm{nbl}}^2(h)} - k^2 - \frac{m^2}{h^2} \right) P_\infty^h - \frac{V_\infty^h}{h} - \frac{mU_\theta \Lambda_{\mathrm{nbl}}(h)}{h^2} V_\infty^h - \left(\frac{(U_\theta^{\mathrm{nbl}})^2}{hc_{\mathrm{nbl}}^2(h)} - \frac{2mU_\theta^{\mathrm{nbl}}}{h^2 \Lambda_{\mathrm{nbl}}(h)} \right) V_\infty^h \right]. \tag{54}
$$

This exactly matches to the term in (34). We then consider the $\mathcal{O}(1)$ terms, which have to sum to zero as $y \to \infty$. Thus, we find that C_h satisfies

$$
\begin{aligned}
& C_h + \frac{\mathrm{i}P_\infty^h}{\rho_{\mathrm{nbl}}(h) c_{\mathrm{nbl}}^2(h)} \int_0^\infty \left(1 - \frac{P_0}{P_\infty^h} \frac{\rho_{\mathrm{nbl}}(h) c_{\mathrm{nbl}}^2(h)}{\widehat{\rho_0} \widehat{c_0}^2}\right) \mathrm{d}y - \mathrm{i}P_\infty^h \frac{k^2 + \frac{m^2}{h^2}}{\rho_{\mathrm{nbl}}(h) \Lambda_{\mathrm{nbl}}^2(h)} \int_0^\infty \left(1 - \frac{P_0}{P_\infty^h} \frac{\rho_{\mathrm{nbl}}(h) \Lambda_{\mathrm{nbl}}^2(h)}{\widehat{\rho_0} \Lambda_h^2}\right) \mathrm{d}y \\
& \quad + \frac{(U_\theta^{\mathrm{nbl}})^2}{hc_{\mathrm{nbl}}^2(h)} \frac{V_\infty^h}{\Lambda_{\mathrm{nbl}}(h)} \int_0^\infty \left(1 - \frac{U_\theta^2 c_{\mathrm{nbl}}^2(h)}{(U_\theta^{\mathrm{nbl}})^2 \widehat{c_0}^2}\right) \mathrm{d}y - \frac{2m\Lambda_h U_\theta^{\mathrm{nbl}}}{h^2 \Lambda_{\mathrm{nbl}}^2(h)} V_\infty^h \int_0^\infty \left(1 - \frac{U_\theta \Lambda_{\mathrm{nbl}}(h)}{U_\theta^{\mathrm{nbl}} \Lambda_h}\right) \mathrm{d}y = 0.
\end{aligned} \tag{55}
$$

2. *Pressure*

We now turn to the pressure component in (53). As $y \to \infty$, we see that the y term is given by

$$
y \left[P_\infty^h \left(\frac{(U_\theta^{\mathrm{nbl}})^2}{hc_{\mathrm{nbl}}^2(h)} - \frac{2mU_\theta^{\mathrm{nbl}}}{h^2 \Lambda_{\mathrm{nbl}}(h)} \right) + \mathrm{i}V_\infty^h \rho_{\mathrm{nbl}}(h) \frac{1}{\Lambda_{\mathrm{nbl}}(h)} \left(\Lambda_{\mathrm{nbl}}^2(h) - 2\frac{(U_\theta^{\mathrm{nbl}})^2}{h^2} \right) \right], \tag{56}
$$

which exactly matches to the term in (35). The $\mathcal{O}(1)$ terms must sum to zero as $y \to \infty$, so D_h satisfies

$$
\begin{aligned}
& D_h - \frac{(U_\theta^{\mathrm{nbl}})^2}{hc_{\mathrm{nbl}}^2(h)} P_\infty^h \int_0^y \left(1 - \frac{P_0}{P_\infty^h} \frac{U_\theta^2 c_{\mathrm{nbl}}^2(h)}{(U_\theta^{\mathrm{nbl}})^2 \widehat{c_0}^2}\right) \mathrm{d}y + \frac{2mU_\theta^{\mathrm{nbl}}}{h^2 \Lambda_{\mathrm{nbl}}(h)} P_\infty^h \int_0^y \left(1 - \frac{P_0}{P_\infty^h} \frac{U_\theta \Lambda_{\mathrm{nbl}}(h)}{U_\theta^{\mathrm{nbl}} \Lambda_h}\right) \mathrm{d}y \\
& \quad + \mathrm{i}\rho_{\mathrm{nbl}}(h) \Lambda_{\mathrm{nbl}}(h) V_\infty^h \int_0^y \left(1 - \frac{\widehat{\rho_0} \Lambda_h^2}{\rho_{\mathrm{nbl}}(h) \Lambda_{\mathrm{nbl}}^2(h)}\right) \mathrm{d}y - 2\mathrm{i} \frac{\rho_{\mathrm{nbl}}(h)(U_\theta^{\mathrm{nbl}})^2}{h^2 \Lambda_{\mathrm{nbl}}(h)} V_\infty^h \int_0^y \left(1 - \frac{\widehat{\rho_0} U_\theta^2}{\rho_{\mathrm{nbl}}(h)(U_\theta^{\mathrm{nbl}})^2}\right) \mathrm{d}y \\
& \quad - \frac{V_\infty^h}{\Lambda_{\mathrm{nbl}}(h)} \int_0^y \mathrm{i}\widehat{\rho_0} \frac{y (U_\theta^2)_y}{h^2} \left(1 - \frac{mU_\theta}{h\Lambda_h} - \frac{(U_\theta^{\mathrm{nbl}})^2}{c_{\mathrm{nbl}}^2(h)}\right) \mathrm{d}y + \int_0^y \frac{\mathrm{i}\widehat{\rho_0} (U_\theta^2)_y}{h\Lambda_h} V_1 \mathrm{d}y = 0.
\end{aligned} \tag{57}
$$

D. Simplifications

Due to the complicated form of both P_1 and V_1, it will be useful to make a simplification before we calculate $P_1(0)$ and $V_1(0)$. For the base flow we note that $\widehat{\rho_0} = \rho_{\text{nbl}} + \mathcal{O}(\delta^\star)$ and $\widehat{c_0} = c_{\text{nbl}} + \mathcal{O}(\delta^\star)$, where $\delta^\star = o(\delta)$. In Figure 1 we see this by plotting the density ratio $\rho_{\text{nbl}}/\widehat{\rho_0}$ (for an exponential boundary layer with displacement thickness $\varepsilon = 0.02$), while the speed of sound ratio is very similar. Since we are only calculating the effective impedance to $\mathcal{O}(\delta)$, then we can approximate the ratios $\rho_{\text{nbl}}/\widehat{\rho_0}$ and $c_{\text{nbl}}^2/\widehat{c_0}^2$ by 1 in (51) and (53). This will be particularly useful in simplifying the pressure term. We refer to this approximation as the "simplified" modified Myers for swirling flow, as opposed to the "full" modified Myers.

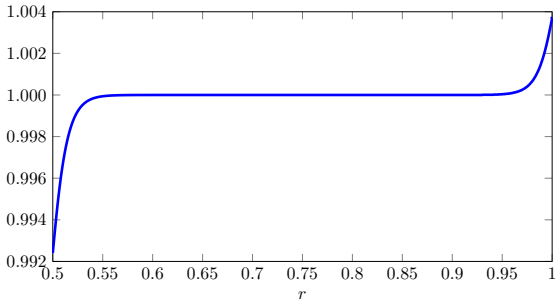

Figure 1: Plot of $\rho_{\text{nbl}}(h)/\widehat{\rho_0}(r)$ showing it can be approximated by a constant for a flow with an exponential boundary layer of displacement thickness $\varepsilon = 0.02$.

E. Solution at the inner duct wall

Finally, we want to calculate $P(0)$ and $V(0)$ at the duct wall, which will then allow us to relate them to the pressure and normal velocity of the flow without a boundary layer at the duct wall, P_∞^h and V_∞^h, and complete the derivation of the modified Myers boundary condition.

1. *Normal velocity*

We have that $V(0) = V_0(0) + \delta V_1(0) + \mathcal{O}(\delta^2)$, which gives

$$V(0) = -\frac{\omega}{\Lambda_{\text{nbl}}(h)} V_\infty^h - \delta\omega C_h + \mathcal{O}(\delta^2). \tag{58}$$

From inserting the expression for $P_0(y)$ from (43) into (55) we calculate C_h and hence find that

$$\begin{aligned}
\frac{V(0)}{V_\infty^h} = &-\frac{\omega}{\Lambda_{\text{nbl}}(h)} + \delta \frac{\mathrm{i}\omega}{\rho_{\text{nbl}}(h) c_{\text{nbl}}^2(h)} \frac{P_\infty^h}{V_\infty^h} \int_0^\infty \left(1 - \frac{\rho_{\text{nbl}}(h) c_{\text{nbl}}^2(h)}{\widehat{\rho_0}\widehat{c_0}^2}\right) \mathrm{d}y \\
&- \delta\mathrm{i} \frac{\omega\left(k^2 + \frac{m^2}{h^2}\right)}{\rho_{\text{nbl}}(h)\Lambda_{\text{nbl}}^2(h)} \frac{P_\infty^h}{V_\infty^h} \int_0^\infty \left(1 - \frac{\rho_{\text{nbl}}(h)\Lambda_{\text{nbl}}^2(h)}{\widehat{\rho_0}\Lambda_h^2}\right) \mathrm{d}y \\
&- \delta \frac{\omega}{h\Lambda_{\text{nbl}}(h)\rho_{\text{nbl}}(h) c_{\text{nbl}}^2(h)} \int_0^\infty \frac{\rho_{\text{nbl}}(h) c_{\text{nbl}}^2(h)}{\widehat{\rho_0}(y)\widehat{c_0}^2(y)} \int_y^\infty \widehat{\rho_0}(y')(U_\theta^2)_{y'} \mathrm{d}y' \mathrm{d}y \\
&+ \delta \frac{\omega\left(k^2 + \frac{m^2}{h^2}\right)}{h\rho_{\text{nbl}}(h)\Lambda_{\text{nbl}}^3(h)} \int_0^\infty \frac{\rho_{\text{nbl}}(h)\Lambda_{\text{nbl}}^2(h)}{\widehat{\rho_0}(y)\Lambda_h^2(y)} \int_y^\infty \widehat{\rho_0}(y')(U_\theta^2)_{y'} \mathrm{d}y' \mathrm{d}y \\
&+ \delta \frac{\omega (U_\theta^{\text{nbl}})^2}{h c_{\text{nbl}}^2(h)\Lambda_{\text{nbl}}(h)} \int_0^\infty \left(1 - \frac{U_\theta^2 c_{\text{nbl}}^2(h)}{(U_\theta^{\text{nbl}})^2 \widehat{c_0}^2}\right) \mathrm{d}y - \delta \frac{2m\omega U_\theta^{\text{nbl}}}{h^2\Lambda_{\text{nbl}}^2(h)} \int_0^\infty \left(1 - \frac{U_\theta \Lambda_{\text{nbl}}(h)}{U_\theta^{\text{nbl}}\Lambda_h}\right) \mathrm{d}y + \mathcal{O}(\delta^2).
\end{aligned} \tag{59}$$

After using the simplification in Section III.D we find the normal velocity is given by

$$\begin{aligned}
\frac{V(0)}{V_\infty^h} = &-\frac{\omega}{\Lambda_{\text{nbl}}(h)} - \delta\mathrm{i} \frac{\omega\left(k^2 + \frac{m^2}{h^2}\right)}{\rho_{\text{nbl}}(h)\Lambda_{\text{nbl}}^2(h)} \frac{P_\infty^h}{V_\infty^h} \int_0^\infty \left(1 - \frac{\Lambda_{\text{nbl}}^2(h)}{\Lambda_h^2}\right) \mathrm{d}y \\
&- \delta \frac{\omega\left(k^2 + \frac{m^2}{h^2}\right)(U_\theta^{\text{nbl}})^2}{h\Lambda_{\text{nbl}}^3(h)} \int_0^y \frac{\Lambda_{\text{nbl}}^2(h)}{\Lambda_h^2} \left[1 - \frac{U_\theta^2}{(U_\theta^{\text{nbl}})^2}\right] \mathrm{d}y - \delta \frac{2m\omega U_\theta^{\text{nbl}}}{h^2\Lambda_{\text{nbl}}^2(h)} \int_0^\infty 1 - \frac{U_\theta \Lambda_{\text{nbl}}(h)}{U_\theta^{\text{nbl}}\Lambda_h} \mathrm{d}y + \mathcal{O}(\delta^2).
\end{aligned} \tag{60}$$

2. Pressure

We have that $P(0) = P_0(0) + \delta P_1(0) + \mathcal{O}(\delta^2)$, and hence

$$\frac{P(0)}{V_\infty^h} = \frac{P_\infty^h}{V_\infty^h} - \frac{\mathrm{i}}{h\Lambda_{\mathrm{nbl}}(h)} \int_0^\infty \widehat{\rho_0}(U_\theta^2)_y \mathrm{d}y + \frac{\delta D_h}{V_\infty^h} + \mathcal{O}(\delta^2). \tag{61}$$

After inserting the definition of $P_0(y)$ and $V_1(y)$ into (57) we calculate D_h. Using the simplifications from Section III.D we then find after a lengthy calculation that

$$\begin{aligned}
\frac{P(0)}{V_\infty^h} = \frac{P_\infty^h}{V_\infty^h} &- \frac{\mathrm{i}}{h\Lambda_{\mathrm{nbl}}(h)} \int_0^\infty \widehat{\rho_0}(U_\theta^2)_y \mathrm{d}y + \delta \frac{\mathrm{i}\rho_{\mathrm{nbl}}(h)(U_\theta^{\mathrm{nbl}})^4}{h^2 c_{\mathrm{nbl}}^2(h)\Lambda_{\mathrm{nbl}}(h)} \int_0^\infty \frac{U_\theta^2}{(U_\theta^{\mathrm{nbl}})^2}\left[1 - \frac{U_\theta^2}{(U_\theta^{\mathrm{nbl}})^2}\right] \mathrm{d}y \\
&- \delta \frac{2mU_\theta^{\mathrm{nbl}}}{h^2\Lambda_{\mathrm{nbl}}(h)} \frac{P_\infty^h}{V_\infty^h} \int_0^\infty 1 - \frac{U_\theta \Lambda_{\mathrm{nbl}}(h)}{U_\theta^{\mathrm{nbl}}\Lambda_h} \mathrm{d}y - \delta \frac{4\mathrm{i}m\rho_{\mathrm{nbl}}(h)(U_\theta^{\mathrm{nbl}})^3}{h^3\Lambda_{\mathrm{nbl}}^2(h)} \int_0^\infty \frac{U_\theta\Lambda_{\mathrm{nbl}}(h)}{U_\theta^{\mathrm{nbl}}\Lambda_h}\left[1 - \frac{U_\theta^2}{(U_\theta^{\mathrm{nbl}})^2}\right] \mathrm{d}y \\
&- \delta\mathrm{i}\rho_{\mathrm{nbl}}(h)\Lambda_{\mathrm{nbl}}(h) \int_0^\infty 1 - \frac{\Lambda_h^2}{\Lambda_{\mathrm{nbl}}^2(h)} \mathrm{d}y + \delta \frac{4\mathrm{i}\rho_{\mathrm{nbl}}(h)(U_\theta^{\mathrm{nbl}})^2}{h^2\Lambda_{\mathrm{nbl}}(h)} \int_0^\infty 1 - \frac{U_\theta^2}{(U_\theta^{\mathrm{nbl}})^2} \mathrm{d}y \\
&+ \frac{\delta\left(k^2 + \frac{m^2}{h^2}\right)(U_\theta^{\mathrm{nbl}})^2}{h\Lambda_{\mathrm{nbl}}^2(h)} \frac{P_\infty^h}{V_\infty^h} \int_0^\infty 1 - \frac{U_\theta^2\Lambda_{\mathrm{nbl}}^2(h)}{(U_\theta^{\mathrm{nbl}})^2\Lambda_h^2} \mathrm{d}y - \frac{2\delta\mathrm{i}m\rho_{\mathrm{nbl}}(h)(U_\theta^{\mathrm{nbl}})^3}{h^3\Lambda_{\mathrm{nbl}}^2(h)} \int_0^\infty 1 - \frac{U_\theta\Lambda_{\mathrm{nbl}}(h)}{U_\theta^{\mathrm{nbl}}\Lambda_h} \mathrm{d}y \\
&+ \frac{\delta\mathrm{i}\left(k^2 + \frac{m^2}{h^2}\right)\rho_{\mathrm{nbl}}(h)(U_\theta^{\mathrm{nbl}})^4}{h^2\Lambda_{\mathrm{nbl}}^3(h)} \int_0^\infty \frac{U_\theta^2\Lambda_{\mathrm{nbl}}^2(h)}{(U_\theta^{\mathrm{nbl}})^2\Lambda_h^2}\left[1 - \frac{U_\theta^2}{(U_\theta^{\mathrm{nbl}})^2}\right] \mathrm{d}y + \mathcal{O}(\delta^2).
\end{aligned} \tag{62}$$

F. The modified Myers boundary condition at the inner wall

Having calculated $P(0)$ and $V(0)$ at the inner wall, we can now compute the effective impedance. We let $Z_h = -P(h)/V(h)$ be the true impedance at the duct wall, and $Z_{\mathrm{eff}} = -P_\infty^h/V_\infty^h$ be the effective impedance needed by the flow without a boundary layer. We now write the bounded integrals in terms of r instead of y. We have that

$$Z_h = -\frac{P(h)}{V(h)} = -\frac{\frac{P(h)}{V_\infty^h}}{\frac{V(h)}{V_\infty^h}} = \frac{Z_{\mathrm{eff}} + \frac{\mathrm{i}}{h\Lambda_{\mathrm{nbl}}(h)} \int_h^{r_m} \widehat{\rho_0}(U_\theta^2)_r \mathrm{d}r - Z_{\mathrm{eff}}^h \delta I_1^h - \delta I_2^h}{-\frac{\omega}{\Lambda_{\mathrm{nbl}}(h)} + Z_{\mathrm{eff}}^h \delta J_1^h + \delta J_2^h} + \mathcal{O}(\delta^2), \tag{63}$$

where

$$\delta J_1^h = \frac{\mathrm{i}\omega\left(k^2 + \frac{m^2}{h^2}\right)}{\rho_{\mathrm{nbl}}(h)\Lambda_{\mathrm{nbl}}^2(h)} \int_h^{r_m} 1 - \frac{\Lambda_{\mathrm{nbl}}^2(h)}{\Lambda_h^2} \mathrm{d}r, \tag{64}$$

$$\delta J_2^h = -\frac{\omega\left(k^2 + \frac{m^2}{h^2}\right)(U_\theta^{\mathrm{nbl}})^2}{h\Lambda_{\mathrm{nbl}}^3(h)} \int_h^{r_m} \frac{\Lambda_{\mathrm{nbl}}^2(h)}{\Lambda_h^2(r)}\left[1 - \frac{U_\theta^2(r)}{(U_\theta^{\mathrm{nbl}})^2}\right] \mathrm{d}r - \frac{2m\omega U_\theta^{\mathrm{nbl}}}{h^2\Lambda_{\mathrm{nbl}}^2(h)} \int_h^{r_m} 1 - \frac{U_\theta\Lambda_{\mathrm{nbl}}(h)}{U_\theta^{\mathrm{nbl}}\Lambda_h} \mathrm{d}r, \tag{65}$$

$$\delta I_1^h = \frac{2mU_\theta^{\mathrm{nbl}}}{h^2\Lambda_{\mathrm{nbl}}(h)} \int_h^{r_m} 1 - \frac{U_\theta\Lambda_{\mathrm{nbl}}(h)}{U_\theta^{\mathrm{nbl}}\Lambda_h} \mathrm{d}r - \frac{\left(k^2 + \frac{m^2}{h^2}\right)(U_\theta^{\mathrm{nbl}})^2}{h\Lambda_{\mathrm{nbl}}^2(h)} \int_h^{r_m} 1 - \frac{U_\theta^2\Lambda_{\mathrm{nbl}}^2(h)}{(U_\theta^{\mathrm{nbl}})^2\Lambda_h^2} \mathrm{d}r, \tag{66}$$

and

$$\begin{aligned}
\delta I_2^h = &\frac{\mathrm{i}\rho_{\mathrm{nbl}}(h)(U_\theta^{\mathrm{nbl}})^4}{h^2 c_{\mathrm{nbl}}^2(h)\Lambda_{\mathrm{nbl}}(h)} \int_h^{r_m} \frac{U_\theta^2}{(U_\theta^{\mathrm{nbl}})^2}\left[1 - \frac{U_\theta^2}{(U_\theta^{\mathrm{nbl}})^2}\right] \mathrm{d}r + \frac{4\mathrm{i}\rho_{\mathrm{nbl}}(h)(U_\theta^{\mathrm{nbl}})^2}{h^2\Lambda_{\mathrm{nbl}}(h)} \int_h^{r_m} 1 - \frac{U_\theta^2}{(U_\theta^{\mathrm{nbl}})^2} \mathrm{d}r \\
&- \mathrm{i}\rho_{\mathrm{nbl}}(h)\Lambda_{\mathrm{nbl}}(h) \int_h^{r_m} 1 - \frac{\Lambda_h^2}{\Lambda_{\mathrm{nbl}}^2(h)} \mathrm{d}r - \frac{4\mathrm{i}m\rho_{\mathrm{nbl}}(h)(U_\theta^{\mathrm{nbl}})^3}{h^3\Lambda_{\mathrm{nbl}}^2(h)} \int_h^{r_m} \frac{U_\theta\Lambda_{\mathrm{nbl}}(h)}{U_\theta^{\mathrm{nbl}}\Lambda_h}\left[1 - \frac{U_\theta^2}{(U_\theta^{\mathrm{nbl}})^2}\right] \mathrm{d}r \\
&+ \frac{\mathrm{i}\left(k^2 + \frac{m^2}{h^2}\right)\rho_{\mathrm{nbl}}(h)(U_\theta^{\mathrm{nbl}})^4}{h^2\Lambda_{\mathrm{nbl}}^3(h)} \int_h^{r_m} \frac{U_\theta^2\Lambda_{\mathrm{nbl}}^2(h)}{(U_\theta^{\mathrm{nbl}})^2\Lambda_h^2}\left[1 - \frac{U_\theta^2}{(U_\theta^{\mathrm{nbl}})^2}\right] \mathrm{d}r \\
&- \frac{2\mathrm{i}m\rho_{\mathrm{nbl}}(h)(U_\theta^{\mathrm{nbl}})^3}{h^3\Lambda_{\mathrm{nbl}}^2(h)} \int_h^{r_m} 1 - \frac{U_\theta\Lambda_{\mathrm{nbl}}(h)}{U_\theta^{\mathrm{nbl}}\Lambda_h} \mathrm{d}r.
\end{aligned} \tag{67}$$

Hence, we calculate that to first order

$$\boxed{Z^h_{\text{eff}} = -\frac{\omega\left(Z_h + \frac{\mathrm{i}}{h\omega}\int_h^{r_m}\widehat{\rho_0}(U_\theta^2)_r \mathrm{d}r\right) + \Lambda_{\text{nbl}}(h)\delta I_2^h + Z_h\Lambda_{\text{nbl}}(h)\delta J_2^h}{\Lambda_{\text{nbl}}(h)\left(1 - \delta I_1^h - Z_h\delta J_1^h\right)}.} \tag{68}$$

G. The modified Myers boundary condition at the outer wall

We can perform very similar analysis at the outer wall to derive the modified Myers boundary condition at $r = 1$. We would make the change of variables $r = 1 - \delta y$ and find both the inner and outer solution by using the same method, and then match them.. Letting $Z_1 = P(1)/V(1)$ and $Z^1_{\text{eff}} = P^1_\infty/V^1_\infty$ we calculate that to first order

$$\boxed{Z^1_{\text{eff}} = \frac{-\omega\left(Z_1 + \frac{\mathrm{i}}{\omega}\int_{r_m}^1\widehat{\rho_0}(U_\theta^2)_r \mathrm{d}r\right) - \Lambda_{\text{nbl}}(1)\delta I_2^d + Z_1\Lambda_{\text{nbl}}(1)\delta J_2^d}{\Lambda_{\text{nbl}}(1)\left(1 + \delta I_1^d - Z_1\delta J_1^d\right)},} \tag{69}$$

where

$$\delta J_1^d = \frac{\mathrm{i}\omega\left(k^2+m^2\right)}{\rho_{\text{nbl}}(1)\Lambda^2_{\text{nbl}}(1)}\int_{r_m}^1 1 - \frac{\Lambda^2_{\text{nbl}}(1)}{\Lambda_1^2}\mathrm{d}r, \tag{70}$$

$$\delta J_2^d = -\frac{\omega\left(k^2+m^2\right)(U_\theta^{\text{nbl}})^2}{\Lambda^3_{\text{nbl}}(1)}\int_{r_m}^1 \frac{\Lambda^2_{\text{nbl}}(1)}{\Lambda_1^2(r)}\left[1 - \frac{U_\theta^2(r)}{(U_\theta^{\text{nbl}})^2}\right]\mathrm{d}r - \frac{2m\omega U_\theta^{\text{nbl}}}{\Lambda^2_{\text{nbl}}(1)}\int_{r_m}^1 1 - \frac{U_\theta\Lambda_{\text{nbl}}(1)}{U_\theta^{\text{nbl}}\Lambda_1}\mathrm{d}r, \tag{71}$$

$$\delta I_1^d = \frac{2mU_\theta^{\text{nbl}}}{\Lambda_{\text{nbl}}(1)}\int_{r_m}^1 1 - \frac{U_\theta\Lambda_{\text{nbl}}(1)}{U_\theta^{\text{nbl}}\Lambda_1}\mathrm{d}r - \frac{\left(k^2+m^2\right)(U_\theta^{\text{nbl}})^2}{\Lambda^2_{\text{nbl}}(1)}\int_{r_m}^1 1 - \frac{U_\theta^2\Lambda^2_{\text{nbl}}(1)}{(U_\theta^{\text{nbl}})^2\Lambda_1^2}\mathrm{d}r, \tag{72}$$

and

$$\begin{aligned}
\delta I_2^d = &-\frac{\mathrm{i}\rho_{\text{nbl}}(1)(U_\theta^{\text{nbl}})^4}{c^2_{\text{nbl}}(1)\Lambda_{\text{nbl}}(1)}\int_{r_m}^1 \frac{U_\theta^2}{(U_\theta^{\text{nbl}})^2}\left[1 - \frac{U_\theta^2}{(U_\theta^{\text{nbl}})^2}\right]\mathrm{d}r - \frac{4\mathrm{i}\rho_{\text{nbl}}(1)(U_\theta^{\text{nbl}})^2}{\Lambda_{\text{nbl}}(1)}\int_{r_m}^1\left[1 - \frac{U_\theta^2}{(U_\theta^{\text{nbl}})^2}\right]\mathrm{d}r \\
&+ \mathrm{i}\rho_{\text{nbl}}(1)\Lambda_{\text{nbl}}(1)\int_{r_m}^1 1 - \frac{\Lambda_1^2}{\Lambda^2_{\text{nbl}}(1)}\mathrm{d}r + \frac{4\mathrm{i}m\rho_{\text{nbl}}(1)(U_\theta^{\text{nbl}})^3}{\Lambda^2_{\text{nbl}}(1)}\int_{r_m}^1 \frac{U_\theta\Lambda_{\text{nbl}}(1)}{U_\theta^{\text{nbl}}\Lambda_1}\left[1 - \frac{U_\theta^2}{(U_\theta^{\text{nbl}})^2}\right]\mathrm{d}r \\
&- \frac{\mathrm{i}\rho_{\text{nbl}}(1)\left(k^2+m^2\right)(U_\theta^{\text{nbl}})^4}{\Lambda^3_{\text{nbl}}(1)}\int_{r_m}^1 \frac{\Lambda^2_{\text{nbl}}(1)U_\theta^2}{\Lambda_1^2(U_\theta^{\text{nbl}})^2}\left(1 - \frac{U_\theta^2}{(U_\theta^{\text{nbl}})^2}\right)\mathrm{d}r \\
&+ \frac{2\mathrm{i}m\rho_{\text{nbl}}(1)(U_\theta^{\text{nbl}})^3}{\Lambda^2_{\text{nbl}}(1)}\int_{r_m}^1\left(1 - \frac{U_\theta\Lambda_{\text{nbl}}(1)}{U_\theta^{\text{nbl}}\Omega_1}\right)\mathrm{d}r,
\end{aligned} \tag{73}$$

with $\Lambda_1(r) = kU_x(r) + mU_\theta(r) - \omega$.

IV. Limit in no swirl

We can check that in the limit of no swirl our effective impedance agrees with the results from Brambley[11] and Khamis & Brambley,[12] which were derived at the outer wall. We have that $\rho_{\text{nbl}}(1) = 1$, $\delta J_2^d = \delta I_1^d = 0$,

$$\delta J_1^d = \frac{\mathrm{i}\omega\left(k^2+m^2\right)}{\Lambda^2_{\text{nbl}}(1)}\int_{r_m}^1 1 - \frac{\Lambda^2_{\text{nbl}}(1)}{\Lambda_1^2}\mathrm{d}r \text{ and } \delta I_2^d = \mathrm{i}\Lambda_{\text{nbl}}(1)\int_{r_m}^1 1 - \frac{\Lambda_1^2}{\Lambda^2_{\text{nbl}}(1)}\mathrm{d}r. \tag{74}$$

The effective impedance is then given by

$$Z^1_{\text{eff}} = \frac{-\omega Z_1 - \Lambda_{\text{nbl}}(1)\delta I_2^d}{\Lambda_{\text{nbl}}(1)\left(1 - Z_1\delta J_1^d\right)}, \tag{75}$$

which agrees exactly with the result in Khamis & Brambley[12] once we account for the different Fourier transform sign convection ($\omega \to -\omega$, $k \to -k$, $m \to -m$).

V. Testing the modified Myers boundary condition in swirl

We now want to show the new boundary condition is behaving as we expect, with quadratic error behaviour with boundary layer thickness. We will compare the exact value of the impedance $Z^1_{\text{eff}} = P_{\text{nbl}}(1)/V_{\text{nbl}}(1)$ with the calculated value from the modified Myers boundary condition in (69), and likewise at the inner wall.

A. Boundary layer profile

We consider a duct where the inner wall is given by $h = 0.5$. We consider an exponential boundary layer profile of

$$L_\alpha(r) = 1 - e^{-\alpha(r-h)} - e^{-\alpha(1-r)}, \tag{76}$$

where we consider different values of α. In Figure 2 we plot the boundary layer profile for $\alpha = 100$, $\alpha = 333$ and $\alpha = 1000$. We define $U_x(r) = U_x^{\text{nbl}} L_\alpha(r)$ and $U_\theta(r) = U_\theta^{\text{nbl}} L_\alpha(r)$. Given a boundary layer profile, the

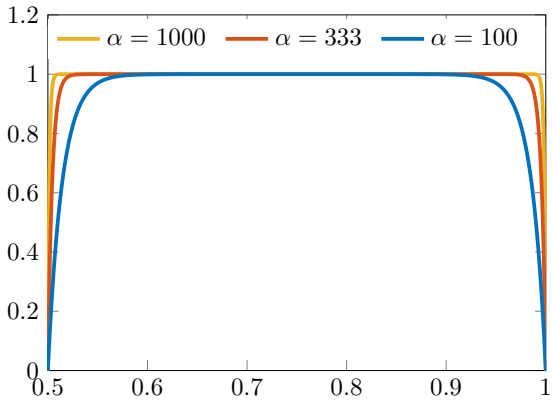

Figure 2: Boundary layer profiles $L_\alpha(r)$ in (76) for different values of α.

displacement thickness is given by

$$\varepsilon^h = 2\int_h^{r_m} 1 - \frac{U_x(r)}{U_x^{\text{nbl}}(r)}\mathrm{d}r \text{ and } \varepsilon^1 = 2\int_{r_m}^1 1 - \frac{U_x(r)}{U_x^{\text{nbl}}(r)}\mathrm{d}r, \tag{77}$$

which is proportional to the boundary layer thickness.

We could instead look at a polynomial or a linear boundary layer to consider laminar boundary layers rather than turbulent boundary layers. However, for these choices of boundary profile, $U_x(r)$ and $U_\theta(r)$ are no longer infinitely differentiable, which makes calculating the eigenmodes harder.

B. Testing the boundary condition at the outer wall

We firstly consider the boundary condition at the outer wall. We consider different values of k, $\omega = 5$, $h = 0.5$, $m = 1$, $U_x^{\text{nbl}} = 0.5$ and $U_\theta^{\text{nbl}} = 0.5$ as a canonical example. We specify an exponential boundary layer profile, but only near $r = 1$. We consider $k = 1$, $k = -1$, $k = 1 + \mathrm{i}$ and $k = -1 - \mathrm{i}$. We choose to set $-P(h)/V(h) = -P_{\text{nbl}}(h)/V_{\text{nbl}}(h) = Z = 1 - \mathrm{i}$, with our choice of Z arbitrary. From using this boundary condition and the governing equations (16) and (22) we can calculate $P_{\text{nbl}}(1)$ and $V_{\text{nbl}}(1)$ by considering a swirling flow with no boundary layer, which allows the exact calculation of Z^1_{eff}. We then solve the same governing equation again but with the swirling flow having the exponential boundary layer, which allows the calculation of $P(1)$ and $V(1)$. We then can compute

$$\boxed{Z^{1,\star}_{\text{eff}} = \frac{-\omega\left(\frac{P(1)}{V(1)} + \frac{\mathrm{i}}{\omega}\int_{r_m}^1 \widehat{\rho_0}(U_\theta^2)_r \mathrm{d}r\right) - \Lambda_{\text{nbl}}(1)\delta I_2^d + \frac{P(1)}{V(1)}\Lambda_{\text{nbl}}(1)\delta J_2^d}{\Lambda_{\text{nbl}}(1)\left(1 + \delta I_1^d - \frac{P(1)}{V(1)}\delta J_1^d\right)},} \tag{78}$$

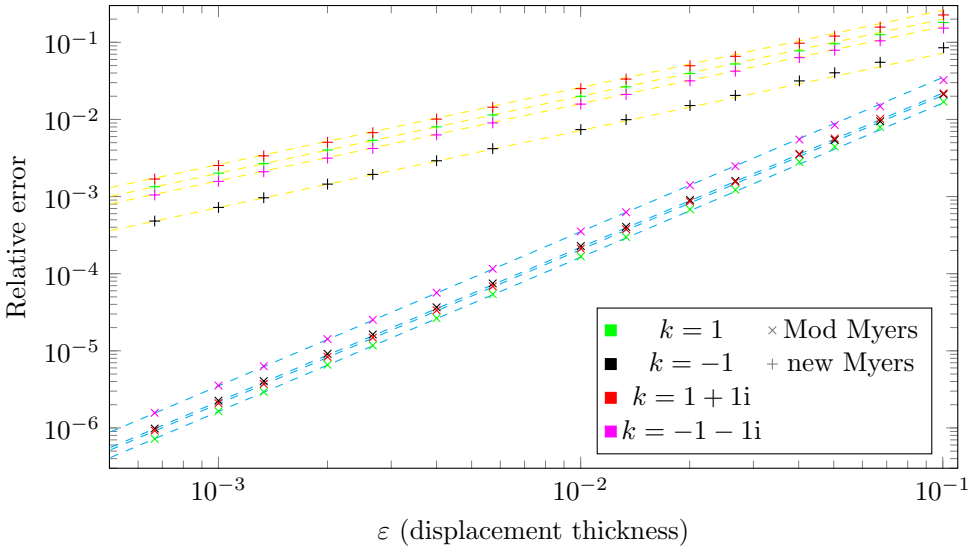

Figure 3: Outer wall. Plot of the relative error of the modified Myers condition $|Z^{1,\star}_{\text{eff}}/Z^{1}_{\text{eff}} - 1|$ (crosses) and corrected Myers condition $|Z^{1,\dagger}_{\text{eff}}/Z^{1}_{\text{eff}} - 1|$ (plusses) against displacement thickness ε. We consider different values of k, $\omega = 5$, $h = 0.5$, $m = 1$, $U^{\text{nbl}}_{x} = 0.5$ and $U^{\text{nbl}}_{\theta} = 0.5$. Yellow dashed lines: gradient 1 (zero order solution); cyan dashed lines: gradient 2 (first order solution).

where δI^{d}_{l} and δJ^{d}_{l} can be found in Section III.G. We then plot the relative error $|Z^{1,\star}_{\text{eff}}/Z^{1}_{\text{eff}} - 1|$ against displacement thickness with crosses in Figure 3. We also consider

$$Z^{1,\dagger}_{\text{eff}} = -\frac{\omega\left(\frac{P(1)}{V(1)} + \frac{\mathrm{i}}{\omega}\int_{r_m}^{1}\widehat{\rho_0}(U^2_\theta)_r \mathrm{d}r\right)}{\Lambda_{\text{nbl}}(1)}, \tag{79}$$

the corrected Myers boundary condition from Masson et al.,[9] and plot the relative error $|Z^{1,\dagger}_{\text{eff}}/Z^{1}_{\text{eff}} - 1|$ against displacement thickness in Figure 3 with plusses. In Figure 3 we see the relative error for the corrected Myers boundary condition is linear as expected (with gradient 1, plotted in yellow). We also see that the relative error for the modified Myers boundary condition is quadratic (with gradient 2, plotted in cyan), which is also as expected.

C. Testing the boundary condition at the inner wall

We can similarly check the modified Myers boundary condition at the inner wall where $h = 0.5$. We use the same parameters as in the previous section, but this time only have a boundary layer profile near $r = h$. We impose a boundary condition at the outer wall of $P(1)/V(1) = P_{\text{nbl}}(1)/V_{\text{nbl}}(1) = Z = 1 - \mathrm{i}$, with Z again arbitrary. From using this boundary condition and the governing equations for swirling flow without a boundary layer we can compute the exact value of $Z^{h}_{\text{eff}} = -P_{\text{nbl}}(h)/V_{\text{nbl}}(h)$. We then consider the swirling flow with a boundary layer and compute $P(h)/V(h)$, which allows us to calculate

$$\boxed{Z^{h,\star}_{\text{eff}} = \frac{-\omega\left(-\frac{P(h)}{V(h)} + \frac{\mathrm{i}}{h\omega}\int_{h}^{r_m}\widehat{\rho_0}(U^2_\theta)_r \mathrm{d}r\right) + \Lambda_{\text{nbl}}(h)\delta I^{h}_{2} - \frac{P(h)}{V(h)}\Lambda_{\text{nbl}}(h)\delta J^{h}_{2}}{\Lambda_{\text{nbl}}(h)\left(1 - \delta I^{h}_{1} + \frac{P(h)}{V(h)}\delta J^{h}_{1}\right)}}, \tag{80}$$

where δI^{h}_{l} and δJ^{h}_{l} are given in Section III.F. We then plot the relative error $|Z^{h,\star}_{\text{eff}}/Z^{h}_{\text{eff}} - 1|$ against displacement thickness with crosses in Figure 4. We also consider

$$Z^{h,\dagger}_{\text{eff}} = \frac{\omega\left(\frac{P(h)}{V(h)} - \frac{\mathrm{i}}{\omega}\int_{h}^{r_m}\widehat{\rho_0}(U^2_\theta)_r \mathrm{d}r\right)}{\Lambda_{\text{nbl}}(h)}, \tag{81}$$

the corrected Myers boundary condition, and plot the relative error $|Z^{h,\dagger}_{\text{eff}}/Z^{h}_{\text{eff}} - 1|$ against displacement thickness in Figure 4 with plusses. We see that the relative error of the corrected Myers boundary condition

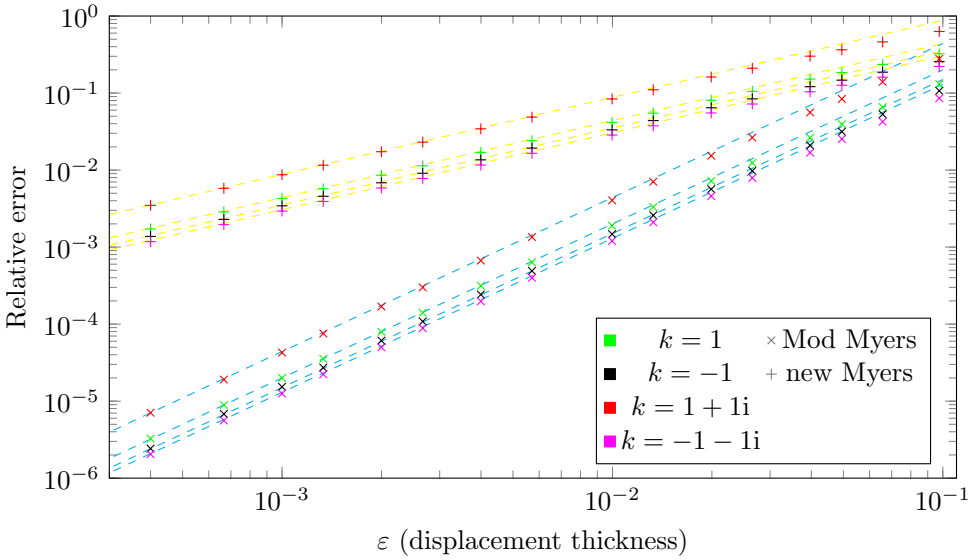

Figure 4: Inner wall. Plot of the relative error of the modified Myers condition $|Z^{h,\star}_{\text{eff}}/Z^{h}_{\text{eff}} - 1|$ (crosses) and corrected Myers condition $|Z^{h,\dagger}_{\text{eff}}/Z^{h}_{\text{eff}} - 1|$ (plusses) against displacement thickness ε. We consider different values of k, $\omega = 5$, $h = 0.5$, $m = 1$, $U^{\text{nbl}}_{x} = 0.5$ and $U^{\text{nbl}}_{\theta} = 0.5$. Yellow dashed lines: gradient 1 (zero order solution); cyan dashed lines: gradient 2 (first order solution).

has the correct linear relationship with displacement thickness, while the relative error of the modified Myers boundary condition has the correct quadratic behaviour.

VI. Extensions and simplifications

We now consider two different situations which makes the results in Section III more useful. We firstly consider the simplification of assuming the boundary layer is linear, before extending the work from Section III to arbitrary varying radial flows.

A. Linear boundary layer

We now consider what happens when we have a linear boundary layer, which allows us to evaluate the integrals δI and δJ analytically. As noted in Khamis & Brambley[12] and Gabard,[10] the shape of the boundary layer is much less significant than the displacement thickness (at least in the case of no swirl). Thus, if the same results holds in swirling flow, for a general boundary layer we could compute the displacement thickness and then emulate the effect of the general boundary layer by using a linear boundary layer with the same displacement thickness.

Let the boundary layer thickness be δ, then we can write

$$U_x(r) = \begin{cases} U^{\text{nbl}}_x (r-h)/\delta & h \le r < h+\delta \\ U^{\text{nbl}}_x & h+\delta \le r < 1-\delta \\ U^{\text{nbl}}_x (1-r)/\delta & 1-\delta \le r \le 1 \end{cases} \text{ and } U_\theta(r) = \begin{cases} U^{\text{nbl}}_\theta (r-h)/\delta & h \le r < h+\delta \\ U^{\text{nbl}}_\theta & h+\delta \le r < 1-\delta \\ U^{\text{nbl}}_\theta (1-r)/\delta & 1-\delta \le r \le 1 \end{cases}. \tag{82}$$

To calculate the eigenvalues we use equations (23) to (26) to give an eigenvalue problem of the form

$$A(U,V,W,P)^T = kB(U,W,W,P)^T, \tag{83}$$

where the matrices A and B are the standard matrices defined in Posson & Peake,[16] Mathews & Peake[17] amongst others. We then have the boundary condition at each duct wall which also depends on k.

1. Non-swirling flow

In Khamis & Brambley[12] it was shown that for non-swirling flow, to first order we get a polynomial in k for the boundary condition of the form

$$P\left[\omega^2 - kU_x\left(2\omega + \mathrm{i}\delta^1 Z_1 m^2\right) + k^2U_x^2 - k^3(\mathrm{i}\delta^1 U_x Z_1)\right] \tag{84}$$
$$- V\left[\omega^2 Z_1 - k\omega U_x\left(Z_1 + \mathrm{i}\delta^1\omega\right) + k^2\frac{5\mathrm{i}\delta^1\omega U_x^2}{3} - k^3\frac{2\mathrm{i}\delta U_x^3}{3}\right] \text{ at } r = 1,$$
$$P\left[\omega^2 - kU_x\left(2\omega + \mathrm{i}\delta^h Z_h(m^2/h^2)\right) + k^2U_x^2 - k^3(\mathrm{i}\delta^h U_x Z_h)\right] \tag{85}$$
$$+ V\left[\omega^2 Z_h - k\omega U_x\left(Z_h + \mathrm{i}\delta^h\omega\right) + k^2\frac{5\mathrm{i}\delta^h\omega U_x^2}{3} - k^3\frac{2\mathrm{i}\delta U_x^3}{3}\right] \text{ at } r = h.$$

To get the hard wall boundary conditions we just take $Z_1, Z_h \to \infty$, while to recover the standard Myers boundary condition in no swirl we set $\delta = 0$. To solve the eigenvalue problem we just define the variables $\dot{P} = kP$, $\ddot{P} = k\dot{P}$, $\dddot{P} = k\ddot{P}$, $\dot{V} = kV$, $\ddot{V} = k\dot{V}$ and $\dddot{V} = k\ddot{V}$ which allows us to remove the eigenvalue from the boundary condition and instead solve the system

$$A^\star(U, V, W, P, \dot{P}, \ddot{P}, \dddot{P}, \dot{V}, \ddot{V}, \dddot{V})^T = kB^\star(U, V, W, P, \dot{P}, \ddot{P}, \dddot{P}, \dot{V}, \ddot{V}, \dddot{V})^T. \tag{86}$$

2. Swirling flow with hard walls

For conciseness, we will only consider the boundary condition at the inner wall. When we have hard walls, we find that by taking $Z_h \to \infty$ in (68) we get

$$Z_{\text{eff}}^h = \frac{\omega + \Lambda_{\text{nbl}}(h)\delta J_2^h}{\Lambda_{\text{nbl}}(h)\delta J_1^h}. \tag{87}$$

We can calculate analytically from the linear boundary layer profile that

$$\delta J_1^h = \delta\frac{\mathrm{i}\left(k^2 + \frac{m^2}{h^2}\right)}{\rho_{\text{nbl}}(h)\Lambda_{\text{nbl}}^2(h)}\left(kU_x^{\text{nbl}} + \frac{mU_\theta^{\text{nbl}}}{h}\right), \tag{88}$$

and

$$\begin{aligned}\delta J_2^h =& \delta\frac{\omega\left(k^2 + \frac{m^2}{h^2}\right)(U_\theta^{\text{nbl}})^2}{h\Lambda_{\text{nbl}}^3(h)}\left(\frac{\Lambda_{\text{nbl}}(h)}{\omega} + \frac{\Lambda_{\text{nbl}}(h)\left[\Lambda_{\text{nbl}}^2(h) - \omega^2 + 2\omega\Lambda_{\text{nbl}}(h)\log\left(-\frac{\Lambda_{\text{nbl}}(h)}{\omega}\right)\right]}{\left(kU_x^{\text{nbl}} + mU_\theta^{\text{nbl}}/h\right)^3}\right)\\ &- \delta\frac{2m\omega^2 U_\theta^{\text{nbl}}}{h^2\Lambda_{\text{nbl}}^2(h)}\frac{1}{(kU_x^{\text{nbl}} + mU_\theta^{\text{nbl}}/h)^2}\left[-\Lambda_{\text{nbl}}(h)\log\left(-\frac{\Lambda_{\text{nbl}}(h)}{\omega}\right) + kU_x^{\text{nbl}} + \frac{mU_\theta^{\text{nbl}}}{h}\right],\end{aligned} \tag{89}$$

so δJ_1^h is a polynomial in k, but δJ_2^h is not, due to the $\log(-\Lambda_{\text{nbl}}(h)/\omega)$ terms. Similar terms to these log terms were found by Khamis & Brambley[12] for the second order modified Myers boundary condition with no swirl. Similar logarithms terms also appear if we consider an exponential boundary layer and calculate the integrals analytically, so they appear to be independent of boundary layer profile.

However, provided our boundary layer is not too large, then we have $|\delta J_2^h| \ll \omega$, and hence the boundary condition becomes approximately

$$Z_{\text{eff}}^h \approx \frac{\omega}{\Lambda_{\text{nbl}}(h)\delta J_1^h} = \frac{\omega h^3\rho_{\text{nbl}}(h)\Lambda_{\text{nbl}}(h)}{\delta\mathrm{i}\left(k^2h^2 + m^2\right)\left(khU_x^{\text{nbl}} + mU_\theta^{\text{nbl}}\right)}, \tag{90}$$

which is a polynomial in k, and we refer to this as the one term modified Myers boundary condition for hard walls in swirling flow. In Table 1 we compare the eigenmodes from a fully resolved boundary layer (second column), the modified Myers boundary condition (third column) and one term modified Myers boundary condition (fourth column), for a low frequency, $\omega = 4$. We can see that there is a noticeable difference between the modified Myers and the one term modified Myers, with the error noticeably larger for the one term modified Myers boundary condition. However, it performs much better than using the standard Myers boundary condition (fifth column), and the polynomial form of the effective impedance means that in general we should use (90) over (87). At higher (and more realistic) frequencies the difference between the modified Myers and the one term modified Myers would decrease, so the boundary condition in (90) becomes even more appealing.

δ	Numerical	Mod Myers	One term MM	Myers
1/100	2.9221	2.9221	2.9223	2.9133
	-3.0772 ± 4.0882i	-3.0765 ± 4.0876i	-3.0800 ± 4.0882i	-3.2254 ± 4.2765i
	-8.7310	-8.7328	-8.7360	-9.1483
1/200	2.9177	2.9177	2.9178	2.9133
	-3.1489 ± 4.1760i	-3.1488 ± 4.1759i	-3.1507 ± 4.1763i	-3.2254 ± 4.2765i
	-8.9228	-8.9232	-8.9247	-9.1483
1/400	2.9155	2.9155	2.9155	2.9133
	-3.1865 ± 4.2245i	-3.1865 ± 4.2245i	-3.1876 ± 4.2247i	-3.2254 ± 4.2765i
	-9.0304	-9.0306	-9.0314	-9.1483

Table 1: Comparison of eigenmodes when $m = -1$, $\omega = 4$, $U_x^{\text{nbl}} = U_\theta^{\text{nbl}} = 0.5$, $h = 0.5$ and hard walls. We compare the eigenmodes from the fully resolved boundary layer, the modified Myers (Eq. (87)), the one term modified Myers (Eq. (90)) and the original Myers boundary condition.

3. Swirling flow with acoustically lined walls

When we have acoustically lined walls, we find that both δI_1^h and δI_2^h have logarithm terms of the form $\log(-\Lambda_{\text{nbl}}(h)/\omega)$ involving k, while we can no longer ignore the δJ_2^h term. Thus, we are unable to get a polynomial in k for Z_{eff}^h, which means we have to solve the eigenvalue problem in a different way, for example by using a numerical dispersion relation.

B. Arbitrary swirling flow profiles

The modified Myers boundary conditions we derived in Section III was only valid for uniform axial and swirling flow. We now show that in fact a very similar result holds for arbitrary swirling flow profiles with a boundary layer, denoted by $U_x(r)$ and $U_\theta(r)$, with $U_x^{\text{nbl}}(r)$ and $U_\theta^{\text{nbl}}(r)$ defining the flow without the boundary layer.

We begin by considering the flow at the inner wall, and use the change of variables $r = h + \delta y$. We define

$$\widehat{U_x}(y) = \frac{U_x^{\text{nbl}}(0)U_x(y)}{U_x^{\text{nbl}}(y)} \text{ and } \widehat{U_\theta}(y) = \frac{U_\theta^{\text{nbl}}(0)U_\theta(y)}{U_\theta^{\text{nbl}}(y)} \tag{91}$$

so that $\widehat{U_x}(y)$ and $\widehat{U_\theta}(y)$ have limits as $y \to \infty$. Upon Taylor expanding (in δ) we find that

$$\frac{U_\theta^{\text{nbl}}(0)}{U_\theta^{\text{nbl}}(y)} = 1 - \delta y \frac{(U_\theta^{\text{nbl}})'(h)}{U_\theta^{\text{nbl}}(h)} + \mathcal{O}(\delta^2) \text{ and } U_\theta(y) = U_\theta(h) + \delta y U_\theta'(h) + \mathcal{O}(\delta^2) = \mathcal{O}(\delta), \tag{92}$$

with the latter following since $U_\theta(h) = 0$. Thus, we get that

$$\widehat{U_\theta}(y) = U_\theta(y) + \mathcal{O}(\delta^2), \tag{93}$$

and similarly

$$\widehat{U_x}(y) = U_x(y) + \mathcal{O}(\delta^2). \tag{94}$$

Thus, to first order we can replace $U_\theta(y)$ by $\widehat{U_\theta}(y)$, $U_x(y)$ by $\widehat{U_x}(y)$ and $\Lambda_h(y)$ by $\widehat{\Lambda_h}(y) = k\widehat{U_x}(y) + m\widehat{U_\theta}(y)/h - \omega$. The effective impedance at the inner wall is then given by

$$Z_{\text{eff}}^h = -\frac{\omega\left(Z_h + \frac{\mathrm{i}}{h\omega}\int_h^{r_m} \widehat{\rho_0}(\widehat{U_\theta}^2)_r \mathrm{d}r\right) + \Lambda_{\text{nbl}}(h)\delta I_2^h + Z_h\Lambda_{\text{nbl}}(h)\delta J_2^h}{\Lambda_{\text{nbl}}(h)\left(1 - \delta I_1^h - Z_h\delta J_1^h\right)}, \tag{95}$$

where the integrands of δI and δJ now involve terms of the form

$$\frac{\widehat{U_\theta}(r)}{U_\theta^{\text{nbl}}(h)} \text{ and } \frac{\widehat{\Lambda_h}(r)}{\Lambda_{\text{nbl}}(h)}, \tag{96}$$

which tend to 1 as $y \to \infty$. We can instead consider the equivalent terms

$$\frac{U_\theta(r)}{U_\theta^{\mathrm{nbl}}(r)} \text{ and } \frac{kU_x(r) + mU_\theta(r)/h - \omega}{kU_x^{\mathrm{nbl}}(r) + mU_\theta^{\mathrm{nbl}}(r)/h - \omega}, \tag{97}$$

with the first following exactly, and the second to leading order, ensuring the fraction still tends to 1 as $y \to \infty$. At the outer wall we find that

$$Z_{\mathrm{eff}}^1 = \frac{-\omega\left(Z_1 + \frac{\mathrm{i}}{\omega}\int_{r_m}^1 \widehat{\rho_0}(\widehat{U_\theta}^2)_r \mathrm{d}r\right) - \Lambda_{\mathrm{nbl}}(1)\delta I_2^d + Z_1\Lambda_{\mathrm{nbl}}(1)\delta J_2^d}{\Lambda_{\mathrm{nbl}}(1)\left(1 + \delta I_1^d - Z_1\delta J_1^d\right)}, \tag{98}$$

where the integrals δI and δJ have an equivalent form.

VII. Eigenmodes and Green's function of realistic SDT flow with a boundary layer

Finally, we consider the modified Myers boundary condition for realistic NASA SDT flow. The mean flow has been extracted from a RANS simulation performed on the NASA SDT test case (Hughes et al.[18] and Woodward et al.[19]) so that the flow is representative of the interstage region between the rotor and stator. This has then been interpolated by a low order Laurent polynomial, with representative non-dimensional axial and swirling flow profiles plotted in Figure 5, with (red) and without (blue) a boundary layer. For convenience we specify an exponential boundary layer. We set $\alpha = 200$ in (76), which gives a displacement thickness of $\varepsilon = 0.01$ for the boundary layer. After non-dimensionalising the SDT flow, we find that representative parameters are $\omega = 15$, $h = 0.5$ and $Z_h = Z_d = 2.55 + 1.5\mathrm{i}$. We will look at two different azimuthal numbers, $m = 1$ and $m = 15$.

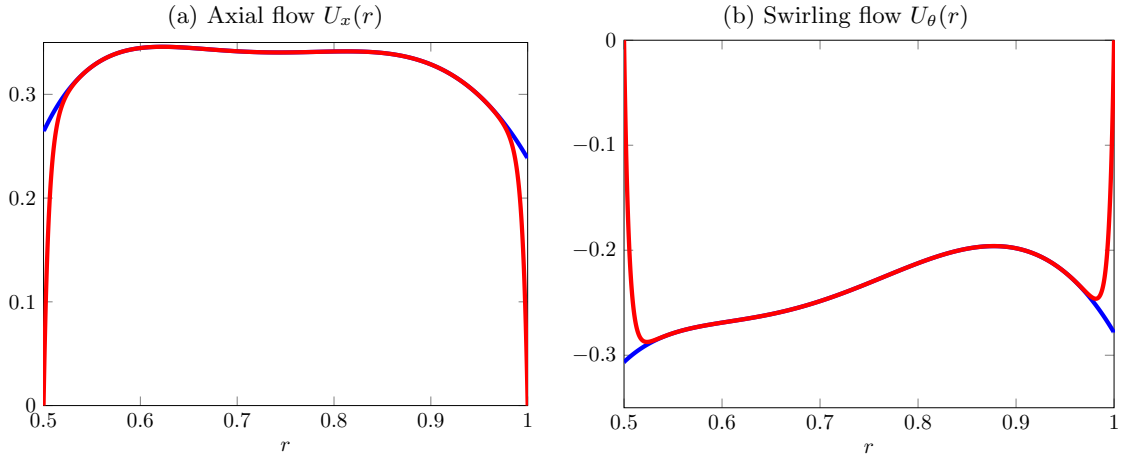

Figure 5: Flow profiles from the SDT data.

We will compare the eigenmodes and Green's function from three different cases. The first will be the flow with the fully resolved boundary layer, so the boundary condition is simply $Z_1 = P(1)/V(1)$ and $Z_h = -P(h)/V(h)$. The second will be with the corrected Myers boundary condition from Masson et al.,[9] so an infinitely thin boundary layer. The third case will be with the modified Myers boundary condition in swirling flow. To compute the eigenmodes and Green's function we will need to use the extension of the modified Myers boundary condition in Section VI.B.

A. Eigenmodes

Since we are unable to write the boundary layer integrals as polynomials in k, the eigenmodes are calculated by solving a numerical dispersion relation, rather than solving a standard eigenvalue problem. Firstly, the eigenmodes for $m = 15$ are computed from the three cases and plotted in Figure 6. The first four upstream and downstream eigenmodes are also given in Table 2 for each of the three cases, and the error from the fully resolved or exact eigenmodes.

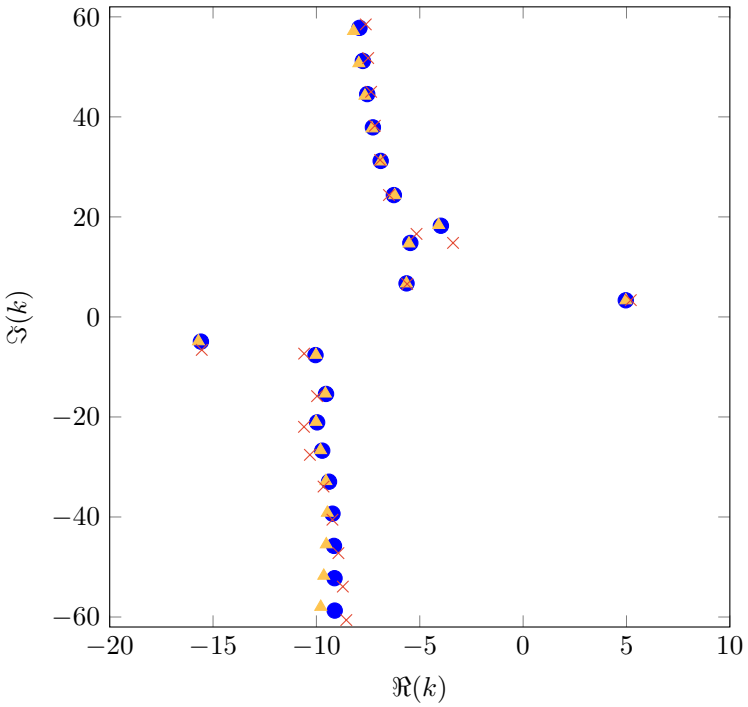

Figure 6: Eigenmodes for the three different cases when $m = 15$, $\omega = 15$, SDT flow, $h = 0.5$ and $Z_j = 2.55 + 1.5\mathrm{i}$. Blue circles: fully resolved boundary layer; Orange triangles: modified Myers; Red crosses: corrected Myers.

In both the table and the figure, using the modified Myers boundary condition gives a much better approximation to the exact eigenmodes for the most cut-on eigenmodes than the corrected Myers boundary condition. In Table 2, the error compared to the exact eigenmode reduces by at least a factor of eight by using the modified Myers boundary condition rather than the Myers boundary condition. It is particularly noticeable in Figure 6 how the third and fourth cut-on downstream eigenmodes (corresponding to the first two lines in Table 2) are much better predicted with the modified Myers boundary condition. Though, as the modes become more cut-off, the modified Myers boundary condition performs less well compared to the exact eigenmodes as shown in Figure 6, but these cut-off eigenmodes are mostly irrelevant for acoustic propagation except maybe close to singularities.

Secondly, the azimuthal mode is set to $m = 1$, while the rest of the problem settings are kept the same. The predicted eigenmodes from the three cases are plotted in Figure 7, and the first four upstream and downstream eigenmodes for the three cases are given in Table 3, with the error compared to the fully resolved boundary layer. The errors are generally smaller than for $m = 15$. The error reduces significantly by using the modified Myers boundary condition rather than the Myers boundary condition, by around a factor

Exact	Mod Myers	$\lvert k_{\text{exact}} - k_{\text{MM}} \rvert$	Myers	$\lvert k_{\text{exact}} - k_{\text{M}} \rvert$
$-3.9780 + 18.2301\mathrm{i}$	$-4.0854 + 18.3725\mathrm{i}$	0.1783	$-5.1567 + 16.6009\mathrm{i}$	2.0110
$-5.4561 + 14.7915\mathrm{i}$	$-5.5221 + 14.6823\mathrm{i}$	0.1276	$-3.3909 + 14.8004\mathrm{i}$	2.0652
$-5.6402 + 6.7034\mathrm{i}$	$-5.6447 + 6.6978\mathrm{i}$	0.0072	$-5.6089 + 6.5779\mathrm{i}$	0.1294
$4.9653 + 3.3240\mathrm{i}$	$4.9672 + 3.3130\mathrm{i}$	0.0112	$5.2080 + 3.3581\mathrm{i}$	0.2451
$-15.5872 - 4.9347\mathrm{i}$	$-15.7070 - 4.8798\mathrm{i}$	0.1317	$-15.5463 - 6.5906\mathrm{i}$	1.6564
$-10.0440 - 7.6305\mathrm{i}$	$-10.0235 - 7.5854\mathrm{i}$	0.0495	$-10.5927 - 7.3347\mathrm{i}$	0.6234
$-9.5334 - 15.3991\mathrm{i}$	$-9.5658 - 15.3288\mathrm{i}$	0.0774	$-9.9681 - 15.8383\mathrm{i}$	0.6180
$-9.9646 - 21.0847\mathrm{i}$	$-10.0199 - 20.9825\mathrm{i}$	0.1163	$-10.6003 - 21.9773\mathrm{i}$	1.0958

Table 2: Comparison of eigenmodes when $m = 15$, $\omega = 15$, SDT flow, $h = 0.5$ and $Z_j = 2.55 + 1.5\mathrm{i}$. We compare the eigenmodes from the fully resolved (or exact) boundary layer, the modified Myers boundary condition and the corrected Myers boundary condition.

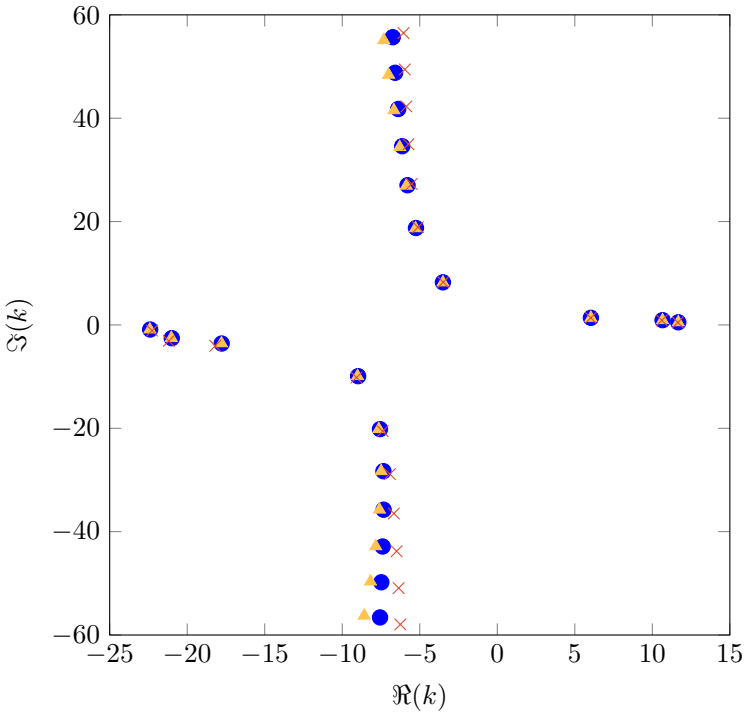

Figure 7: Eigenmodes for the three different cases when $m = 1$, $\omega = 15$, SDT flow, $h = 0.5$ and $Z_j = 2.55 + 1.5\mathrm{i}$. Blue circles: fully resolved boundary layer; Orange triangles: modified Myers; Red crosses: corrected Myers.

of eight again except for the fourth downstream eigenmode (the first line in the table). For this mode, using the modified Myers boundary condition does not bring much improvement compared to the Myers boundary condition, with the reason probably down to one error cancelling another error (e.g. first and second order errors) when using the Myers boundary condition. In Figure 7, again, the modified Myers boundary condition performs less well for the more cut-off eigenmodes, and in some cases is not more accurate than using the Myers boundary condition.

Exact	Mod Myers	$\lvert k_{\text{exact}} - k_{\text{MM}}\rvert$	Myers	$\lvert k_{\text{exact}} - k_{\text{M}}\rvert$
$-3.5077 + 8.2416\mathrm{i}$	$-3.5070 + 8.2209\mathrm{i}$	0.0208	$-3.4886 + 8.2674\mathrm{i}$	0.0321
$6.0372 + 1.3762\mathrm{i}$	$6.0356 + 1.3747\mathrm{i}$	0.0021	$6.0293 + 1.3632\mathrm{i}$	0.0152
$10.6597 + 0.9225\mathrm{i}$	$10.6583 + 0.9235\mathrm{i}$	0.0017	$10.6121 + 0.8940\mathrm{i}$	0.0554
$11.6745 + 0.5079\mathrm{i}$	$11.6735 + 0.5091\mathrm{i}$	0.0015	$11.6430 + 0.4822\mathrm{i}$	0.0407
$-22.3894 - 0.8848\mathrm{i}$	$-22.4104 - 0.8795\mathrm{i}$	0.0216	$-22.2694 - 1.0990\mathrm{i}$	0.2455
$-20.9954 - 2.5591\mathrm{i}$	$-21.0231 - 2.5213\mathrm{i}$	0.0468	$-21.1882 - 3.0957\mathrm{i}$	0.5702
$-17.7767 - 3.5975\mathrm{i}$	$-17.7895 - 3.5589\mathrm{i}$	0.0406	$-18.1950 - 4.0476\mathrm{i}$	0.6145
$-8.9760 - 9.9158\mathrm{i}$	$-9.0110 - 9.9037\mathrm{i}$	0.0371	$-9.0795 - 10.1830\mathrm{i}$	0.2866

Table 3: Comparison of eigenmodes when $m = 1$, $\omega = 15$, SDT flow, $h = 0.5$ and $Z_j = 2.55 + 1.5\mathrm{i}$. We compare the eigenmodes from the fully resolved boundary layer, the modified Myers boundary condition and the corrected Myers boundary condition.

B. Acoustic Green's function

As in Posson & Peake,[16] it is then possible to compute the Green's function, for the acoustic analogy defined by (11), that is tailored to the duct with the chosen boundary conditions. The reduced Green's function $\widehat{p}_\omega$, which satisfies

$$\mathcal{F}\left(\widehat{p}_\omega(\boldsymbol{x}|\boldsymbol{x}_0)e^{-\mathrm{i}\omega t}\right) = \frac{1}{2\pi}\frac{D_0^2}{Dt^2}\mathcal{R}\left(\delta(\boldsymbol{x}-\boldsymbol{x}_0)e^{-\mathrm{i}\omega t}\right). \tag{99}$$

is given by

$$\widehat{p}_\omega(\boldsymbol{x}|\boldsymbol{x}_0) = \frac{1}{4\pi^2}\sum_{m=-\infty}^{\infty} e^{\mathrm{i}m(\theta-\theta_0)}\int_{\mathbb{R}}\widehat{p}_m(r|r_0;\omega,k)e^{\mathrm{i}k(x-x_0)}\mathrm{d}k, \tag{100}$$

with

$$\widehat{p}_m(r|r_0;\omega,k) = \frac{1}{2\pi r_0\mathcal{W}(r_0,k)}\begin{cases} g_1(r_0;k)g_2(r;k) & r\le r_0 \\ g_2(r_0;k)g_1(r;k) & r>r_0 \end{cases}, \tag{101}$$

where $\mathcal{W}(r_0,k)$ is the Wrońskian of $g_1(r;k)$ and $g_2(r;k)$, which both satisfy (16). The function $g_1(r;k)$ satisfies the appropriate boundary condition at $r=1$ and $g_2(r;k)$ satisfies the boundary condition at $r=h$. We could also consider the more standard reduced Green's function G_ω which satisfies $\mathcal{F}\left(G_\omega(\boldsymbol{x}|\boldsymbol{x}_0)e^{-\mathrm{i}\omega t}\right) = \delta(\boldsymbol{x}-\boldsymbol{x}_0)e^{-\mathrm{i}\omega t}$, as in Mathews & Peake.[17]

To evaluate the Green's function, the contour in (100) is deformed in accordance with the Briggs-Bers[5,20,21] procedure. This new contour is then closed in the upper or lower half plane, depending on the sign of $x-x_0$. When $x-x_0>0$, it is closed in the upper half plane, which gives a sum of residues at the acoustic downstream modes plus an integral around the critical layer and hydrodynamic modes, while if $x-x_0<0$, it is closed in the lower half plane and just gives a sum of residues at the acoustic upstream modes. The contribution from the critical layer and the hydrodynamic modes has been shown to be considerably smaller than the contribution from the acoustic modes,[16] so their contribution will be ignored from this integral as it is computationally expensive.

After evaluating the residues, the contribution from each azimuthal number reads

$$\widehat{p}^m_\omega(r,x|r_0,x_0) = \pm\sum_{\mathcal{K}^\pm_m}\frac{\mathrm{i}\omega}{4\pi^2}e^{\mathrm{i}k^n_m(x-x_0)}\frac{1}{r_0\frac{\partial\mathcal{W}}{\partial k}(k^n_m)}\begin{cases} g_1(r_0;k^n_m)g_2(r;k^n_m) & r\le r_0 \\ g_2(r_0;k^n_m)g_1(r;k^n_m) & r>r_0 \end{cases}, \tag{102}$$

where the $\pm$ comes from the sign of $x-x_0$, $\mathcal{K}^+_m$ consists of all downstream acoustic modes, $\mathcal{K}^-_m$ consists of all upstream acoustic modes, and the acoustic modes are indexed by n. The Green's function $\widehat{p}_\omega$ is then calculated as Fourier summing $\widehat{p}^m_\omega$.

The Green's function contribution of the two azimuthal numbers $m=1$ and $m=15$ is computed, plotting both the upstream and downstream Green's function for the source position $r_0=0.75$ and $x-x_0=\pm1$. The method for calculating the Green's function is the same as in Posson & Peake[16] or Mathews & Peake,[16] but with the new boundary condition.

Firstly, the contributions of the mode $m=15$ to both the upstream and the downstream Green's function are plotted in Figure 8. The different colours correspond to the choice of boundary condition, while the solid line corresponds to $\Re(\widehat{p}^m_\omega)$ and the dashed line $\Im(\widehat{p}^m_\omega)$. Using the corrected Myers boundary condition (red)

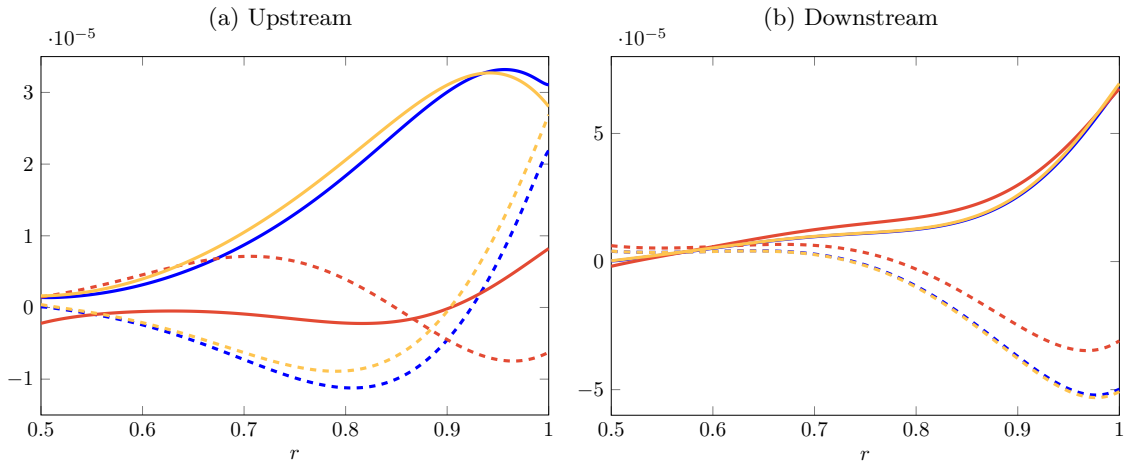

Figure 8: Upstream and downstream acoustic Green's function $\widehat{p}^m_\omega(r,x|r_0,x_0)$ for $m=15$. Blue: exact boundary condition; orange: modified Myers boundary condition; red: corrected Myers condition. Solid: real part; dashed: imaginary part. Source is at $(r_0,x-x_0)=(0.75,\pm1)$.

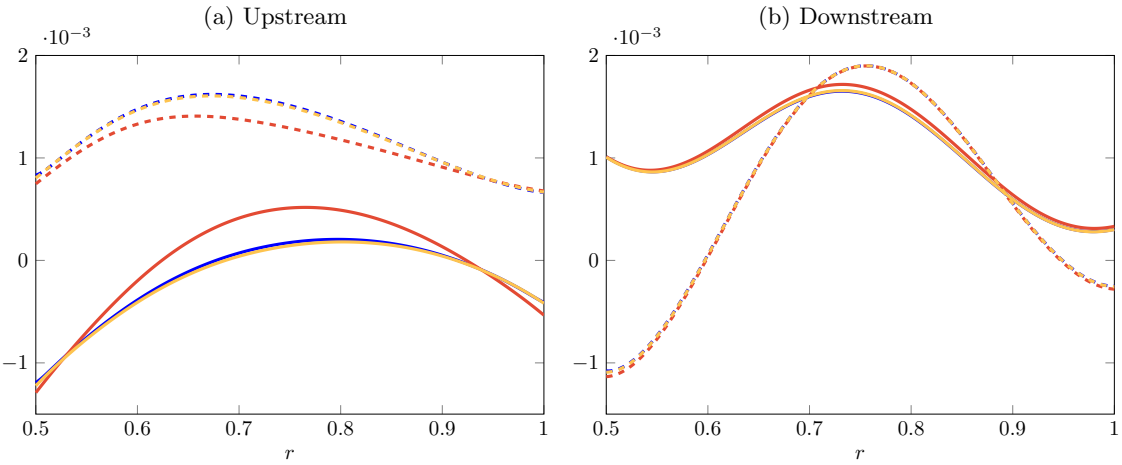

Figure 9: Upstream and downstream acoustic Green's function $\widehat{p}^m_\omega(r, x|r_0, x_0)$ for $m = 1$. Blue: exact boundary condition; orange: modified Myers boundary condition; red: corrected Myers condition. Solid: real part; dashed: imaginary part. Source is at $(r_0, x - x_0) = (0.75, \pm 1)$.

is a really poor approximation compared to the fully resolved boundary layer (blue) for the upstream Green's function, with the Green's function having completely different behaviour throughout the duct. If instead the modified Myers boundary condition (orange) is used the approximation is much more accurate, and gives the correct shape of the upstream Green's function, although the amplitude of the Green's function differs by a small amount. The cause of the large discrepancy of the Myers boundary condition is the huge error in determining the most cut-on upstream eigenmode in Table 2 when using the Myers boundary condition.

In contrast, the downstream Green's function in Figure 8b is significantly less affected by the boundary condition. The modified Myers boundary condition performs extremely well compared to the fully resolved boundary layer, with the difference hardly visible in Figure 8b. Using the corrected Myers boundary condition instead makes the Green's function less accurate, but it still has the same qualitative behaviour as the Green's function from the fully resolved boundary layer.

Secondly, the contributions of the mode $m = 1$ to both the upstream and the downstream Green's function are plotted in Figure 9. Similar behaviour as for the mode $m = 15$ is observed. Namely the upstream Green's function is significantly more affected by the boundary condition than the downstream Green's function. However, the discrepancies of both predictions with the modified Myers boundary condition and the Myers boundary condition are much more reduced for $m = 1$ than for $m = 15$. The downstream prediction from the modified Myers boundary condition is indistinguishable from that predicted with the fully resolved boundary layer in Figure 9b, while using the Myers boundary condition only produces a very small error. For the upstream Green's function in Figure 9a, using the modified Myers boundary condition gives a Green's function which is very accurate when compared to the fully resolved boundary layer. The corrected Myers boundary condition performs a lot better than when $m = 15$ but there is still a significant error in the interior of the duct when compared with the exact solution.

VIII. Conclusion

In this paper, a new modified Myers boundary condition for swirling flow, which accounts for the fact that the base flow in an annular duct has a small but non-zero boundary layer due to viscous effects has been derived. This boundary condition was initially derived for a uniform axial and swirling flow profile, before being extended to arbitrary swirling flow profiles. It was shown that in the limit of zero swirl, the boundary condition reduced to that given in Brambley[11] and Khamis & Brambley,[12] while it performs much better than the corrected Myers boundary condition detailed in Masson et al.,[9] with a quadratic error $\mathcal{O}(\delta^2)$ rather than linear error $\mathcal{O}(\delta)$ compared to the boundary layer thickness δ.

Finally, the new modified Myers boundary condition was used to calculate the eigenmodes and Green's function for a realistic flow, corresponding to the NASA SDT interstage flow at approach condition. It was shown that it was essential in some cases (especially when the observer is upstream of the source) to use the new boundary condition rather than the corrected Myers boundary condition to have the correct eigenmode

and Green's function behaviour.

Acknowledgements

James Mathews was funded by ENOVAL, grant number MMZC/084 RG70800. The authors would like to thank Dr. Ed Brambley, Dr. Doran Khamis and Pr. Nigel Peake from the University of Cambridge as well as Pr. Michel Roger from École Centrale de Lyon, for the interesting conversations about this topic and their precious advice. Doran Khamis suggested the inner solution scaling in (39). The authors are also grateful to Thomas Nodé-Langlois from Airbus for having provided the RANS data for the SDT test case.

References

[1]ACARE, "Strategic Research Agenda: Volume 1," `http://www.acare4europe.com/sites/acare4europe.org/files/attachment/SRIA%20Volume%201.pdf`, 2002, [Online; accessed 07-April-2017].

[2]Flightpath, "Europe's Vision for Aviation: Maintaining Global Leadership & Serving Society's Needs," `http://ec.europa.eu/transport/modes/air/doc/flightpath2050.pdf`, 2011, [Online; accessed 07-April-2017].

[3]Myers, M., "On the acoustic boundary condition in the presence of flow," *Journal of Sound and Vibration*, Vol. 71, No. 3, 1980, pp. 429–434.

[4]Ingard, U., "Influence of fluid motion past a plane boundary on sound reflection, absorption, and transmission," *The Journal of the Acoustical Society of America*, Vol. 31, No. 7, 1959, pp. 1035–1036.

[5]Brambley, E. J., "Fundamental problems with the model of uniform flow over acoustic linings," *Journal of Sound and Vibration*, Vol. 322, No. 4, 2009, pp. 1026–1037.

[6]Renou, Y. and Aurégan, Y., "Failure of the Ingard–Myers boundary condition for a lined duct: An experimental investigation," *The Journal of the Acoustical Society of America*, Vol. 130, No. 1, 2011, pp. 52–60.

[7]Eversman, W. and Beckemeyer, R. J., "Transmission of sound in ducts with thin shear layersconvergence to the uniform flow case," *The Journal of the Acoustical Society of America*, Vol. 52, No. 1B, 1972, pp. 216–220.

[8]Tester, B. J., "Some aspects of sound attenuation in lined ducts containing inviscid mean flows with boundary layers," *Journal of Sound and Vibration*, Vol. 28, No. 2, 1973, pp. 217–245.

[9]Masson, V., Mathews, J. R., Sanjose, M., Moreau, S., and Posson, H., "Liner behavior in an annular duct with swirling and sheared mean flow," *23rd AIAA/CEAS Aeroacoustics Conference, Denver*, 2017.

[10]Gabard, G., "A comparison of impedance boundary conditions for flow acoustics," *Journal of Sound and Vibration*, Vol. 332, No. 4, 2013, pp. 714–724.

[11]Brambley, E. J., "Well-posed boundary condition for acoustic liners in straight ducts with flow," *AIAA journal*, Vol. 49, No. 6, 2011, pp. 1272–1282.

[12]Khamis, D. and Brambley, E. J., "Acoustic boundary conditions at an impedance lining in inviscid shear flow," *Journal of Fluid Mechanics*, Vol. 796, 2016, pp. 386–416.

[13]Rienstra, S. W. and Darau, M., "Boundary-layer thickness effects of the hydrodynamic instability along an impedance wall," *Journal of Fluid Mechanics*, Vol. 671, 2011, pp. 559–573.

[14]Myers, M. and Chuang, S., "Uniform asymptotic approximations for duct acoustic modes in a thin boundary-layer flow," *AIAA journal*, Vol. 22, No. 9, 1984, pp. 1234–1241.

[15]Joubert, L., *Asymptotic approach for the mathematical and numerical analysis of the acoustic propagation in a strong shear flow*, Ph.D. thesis, PhD thesis, École Polytechnique (in French), 2010.

[16]Posson, H. and Peake, N., "The acoustic analogy in an annular duct with swirling mean flow," *Journal of Fluid Mechanics*, Vol. 726, 2013, pp. 439–475.

[17]Mathews, J. R. and Peake, N., "The acoustic Green's function for swirling flow in a lined duct," *Journal of Sound and Vibration*, Vol. 395, 2017, pp. 294–316.

[18]Hughes, C., Jeracki, R., Woodward, R., and Miller, C., "Fan noise source diagnostic test-rotor alone aerodynamic performance results," *8th AIAA/CEAS Aeroacoustics Conference, Breckenridge, Colorado*, 2002.

[19]Woodward, R., Hughes, C., Jeracki, R., and Miller, C., "Fan Noise Source Diagnostic Test–Far-field Acoustic Results," *8th AIAA/CEAS Aeroacoustics Conference, Breckenridge, Colorado*, 2002.

[20]Briggs, R. J., *Electron-stream interaction with plasmas*, MIT Press, 1964.

[21]Bers, A., "Space-time evolution of plasma instabilities-absolute and convective," *Basic plasma physics, Volume 1*, 1983.